The Paton WELDING JOURNAL

April 2000 # 4

English translation of the monthly «Avtomaticheskaya Svarka» journal published in Russian since 1948

«The Paton Welding Journal» monthly is published by the E.O. Paton Electric Welding Institute of the National Academy of Sciences of Ukraine with the support rendered by the International Association «Welding».

Promotion group:
V.N.Lipodaev, V.I.Lokteva
A.T.Zelnichenko (Exec. director)

Editorial and advertising offices are located at PWI, Dept. 51, 11, Bozhenko str., 252650, Kyiv, Ukraine.
Tel.: (38044) 227 67 57
Fax: (38044) 268 04 86
E-mail: paton@i.kiev.ua; paton@iptelecom.net.ua

Subscriptions:
$460, 12 issues

«The Paton Welding Journal» Website: http://www.nas.gov.ua/pwj

CONTENTS

SPACE TECHNOLOGIES ON THE THRESHOLD OF THE THIRD MILLENIUM

B.E. PATON
The E.O. Paton Electric Welding Institute, NASU, Kyiv, Ukraine

ABSTRACT

Promising trends in development of space technologies in the next decades are discussed. Special attention is given to comprehensive material science research.

Key words: *industrialisation of space, space technologies, material science, international integration.*

Yury Gagarin's flight into space in April, 1961, has certainly become one of the major events of the elapsing millennium, which actually marked the start of the era of the man mastering the near-the-earth space. Going beyond the limits of gravity pull was due not only to the desire to learn the unknown inherent to man, but also to the search for new additional energy resources, as well as the ability to use the specific conditions of space for a successful solution of various applied and scientific problems. By the start of the 1970s some practical tasks had already been solved, namely production of the pictures of atmospheric phenomena, performance of diagnostics of mineral deposits, establishment of satellite communications, etc. More over, the results of medico-biological experiments in numerous manned flights confirmed the possibility of human activity in space. With the start of functioning of «Salyut» and «Skylab» space stations in the near-the-earth orbit, it became possible to conduct systematic studies of the near space atmosphere, space and process experiments under zero-gravity conditions, as well as monitor the surface of the Earth, etc. Solving quite a number of problems related to human activity in space, was required simultaneously:

erection of large-sized structures in orbit;

construction of long-endurance space stations and providing them with power resources;

performance of exstravehicular activity (EVA) by the cosmonauts when servicing the space objects;

use of lunar resources in the interests of the national economy;

industrialization of space, in particular, taking environmentally polluting productions into orbit;

lighting of northern regions, creation of additional sources of energy, satellite communications, etc.;

use of near-the-earth orbit as the starting orbit in interplanetary flights;

solving the «space debris» problem.

This will certainly require several decades and depends not only on the level of technical development of the space industry, its creative potential, but also on financial support of the scientific and technical programs being developed. Despite the fact that the combination of these factors was not always favourable over the past years, cosmonautics has still achieved considerable success. Expansion of the programs related to construction in space of long-endurance orbital space stations (OSS) and of large-sized structures, necessitated the implementation of concrete highly specialized technologies in orbit (assembly, mounting, welding, cutting, brazing, etc.). The very first welding experiment conducted in space in 1969, initiated a new trend in the field of process development, namely space technologies.

The range of technological processes conducted in orbit has become much wider since then, while space technology formed its own areas of biotechnology, agrotechnology, etc., whose number will increase, as the problems facing the researchers become more profound and broader. However, significant achievements of the production aspect of space technology can already be noted. The main spectrum of processing operations in this area which have been conducted in near-the-earth orbit over the last 30 years and have found concrete implementation in the hardware, is given in the Figure.

The systemic approach to solving the priority problems of the space industry, allowed the «Mir» orbital complex to be created in a short time by the start of the 1980s through the efforts of the leading experts. The long-term operation of this complex was a prerequisite for a successful performance of process experiments and research in the field of material science, fundamental physics, astronomy, etc.

The unique properties of space (microgravity, superpure dynamic vacuum, low and high temperatures, unusual radiation situation) opened up great

SPACE TECHNOLOGIES ON THE THRESHOLD OF THE THIRD MILLENIUM

B.E. PATON
The E.O. Paton Electric Welding Institute, NASU, Kyiv, Ukraine

ABSTRACT

Promising trends in development of space technologies in the next decades are discussed. Special attention is given to comprehensive material science research.

Key words: *industrialisation of space, space technologies, material science, international integration.*

Yury Gagarin's flight into space in April, 1961, has certainly become one of the major events of the elapsing millennium, which actually marked the start of the era of the man mastering the near-the-earth space. Going beyond the limits of gravity pull was due not only to the desire to learn the unknown inherent to man, but also to the search for new additional energy resources, as well as the ability to use the specific conditions of space for a successful solution of various applied and scientific problems. By the start of the 1970s some practical tasks had already been solved, namely production of the pictures of atmospheric phenomena, performance of diagnostics of mineral deposits, establishment of satellite communications, etc. More over, the results of medico-biological experiments in numerous manned flights confirmed the possibility of human activity in space. With the start of functioning of «Salyut» and «Skylab» space stations in the near-the-earth orbit, it became possible to conduct systematic studies of the near space atmosphere, space and process experiments under zero-gravity conditions, as well as monitor the surface of the Earth, etc. Solving quite a number of problems related to human activity in space, was required simultaneously:

erection of large-sized structures in orbit;

construction of long-endurance space stations and providing them with power resources;

performance of exstravehicular activity (EVA) by the cosmonauts when servicing the space objects;

use of lunar resources in the interests of the national economy;

industrialization of space, in particular, taking environmentally polluting productions into orbit;

lighting of northern regions, creation of additional sources of energy, satellite communications, etc.;

use of near-the-earth orbit as the starting orbit in interplanetary flights;

solving the «space debris» problem.

This will certainly require several decades and depends not only on the level of technical development of the space industry, its creative potential, but also on financial support of the scientific and technical programs being developed. Despite the fact that the combination of these factors was not always favourable over the past years, cosmonautics has still achieved considerable success. Expansion of the programs related to construction in space of long-endurance orbital space stations (OSS) and of large-sized structures, necessitated the implementation of concrete highly specialized technologies in orbit (assembly, mounting, welding, cutting, brazing, etc.). The very first welding experiment conducted in space in 1969, initiated a new trend in the field of process development, namely space technologies.

The range of technological processes conducted in orbit has become much wider since then, while space technology formed its own areas of biotechnology, agrotechnology, etc., whose number will increase, as the problems facing the researchers become more profound and broader. However, significant achievements of the production aspect of space technology can already be noted. The main spectrum of processing operations in this area which have been conducted in near-the-earth orbit over the last 30 years and have found concrete implementation in the hardware, is given in the Figure.

The systemic approach to solving the priority problems of the space industry, allowed the «Mir» orbital complex to be created in a short time by the start of the 1980s through the efforts of the leading experts. The long-term operation of this complex was a prerequisite for a successful performance of process experiments and research in the field of material science, fundamental physics, astronomy, etc.

The unique properties of space (microgravity, superpure dynamic vacuum, low and high temperatures, unusual radiation situation) opened up great

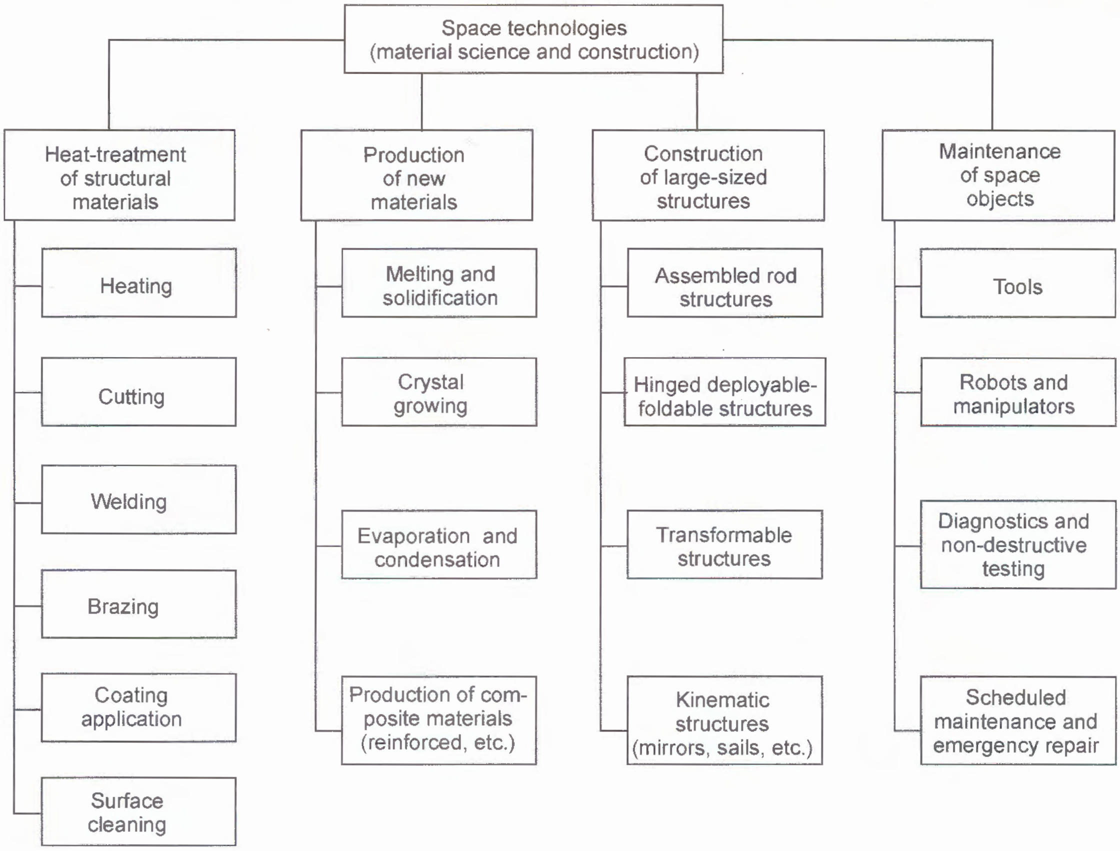

prospects for production of materials with a more perfect than on the Earth, structure and better physico-chemical and mechanical properties. Therefore, it is natural that the attention of space material science in the initial period of research performance is focused on investigation the phenomena which obviously depend on gravity and have been quite well studied on the Earth, namely heat and mass transfer, diffusion, surface tension and wettability, capillary phenomena, phases formation, melting and solidification, growth of single-crystals, etc. The result of this fundamental research was determination of the possibility of production of materials with unique properties difficult to achieve (or even unachievable) on the Earth. Among the main kinds of products whose fabrication under the space conditions can be rational and cost effective, the following should be named:

structurally-perfect semi-conductor single-crystals of a high purity and large dimensions;

eutectic alloys consisting of two components differing in their composition and properties, with unlimited mutual solubility in the molten state and insignificant solubility in the solid state;

high-strength high-temperature foam materials with a low specific weight;

superhard metal alloys with greatly different densities of their components;

optically transparent materials;

metal alloys having an area of immiscibility in the liquid state or alloys with non-uniform nucleation;

composite materials of the type of metal–metal, metal–metal oxide, ceramic and organic substances which do not mix on the Earth;

various coatings for the optical and electronic industry.

Improvement of the properties of materials (electrical resistance, magnetic susceptibility, mechanical strength, permeance, structural perfection, etc.) produced in space, is due to reduction of convection and mass transfer, higher dispersion of the phases, absence of sedimentation, presence of the diffusion mechanism of melt homogenizing in solidification, uniform mixing of gases with metals and of components immiscible on the Earth, possibility of conducting crucibleless melting in a cleaner vacuum atmosphere. Intensive development of space material science in the new millennium is only possible if perfect equipment and advanced research procedures are used, such as, for instance, displays of nucleation, growth and coalescence in immiscible alloys, using X-ray devices, monitoring the growth rate with fluxmeters, temperature stabilization using thermal tubes, temperature and convection monitoring in infrared radiation, various methods of levitation of liquid volumes, etc.

The long-term (approximately 25 to 30 years) operation of OSS involving inevitable damage of the structure and failures of equipment, implies the ability of conducting effective and safe EVA by the cosmonauts. The programs of planning and engineering-technical preparation for EVA include OSS maintenance and repair, assembly-mounting work and provision of normal functioning of the scientific hardware located on the outer surface of the space station. When the above operations are performed in raw space, robots, automatic and controllable manipulators, various devices for cosmonauts' movement outside the station, can be used.

The current stage of development of cosmonautics is associated with the era of space optimization. An intensive process of international integration and organizing joint space programs is observed against the background of the world crisis phenomena. The already started construction of the International Space Station is an example of international cooperation in the space industry. Creation of large scientific-technological laboratories in orbit will expand the prospects for study of new states of the matter (ultra-microparticles, plasma-crystals, etc.), which is only possible at microgravity. Further progress of those areas of cosmonautics which already now yield real profit, will lead to creation of global networks of communication, TV, information, weather forecasting, navigation, Earth's nature monitoring, etc. Close is the time when large-scale productions vitally important for humanity, will be deployed in near-the-earth orbits. Powerful space energy generation systems, namely space solar power stations which will make a significant contribution to power generation on the Earth, should become the necessary basis for space industrialization. It is intended to perform power transmission through the radio beam which easily passes through the atmosphere and is guided to the terrestrial receiving aerial by special means. Perfection of the means of payload delivery to orbit, creation of an ergonomic system of transportation in orbit proper, will allow setting up permanent lunar outposts and using its resources for the needs of terrestrial production. Mastering of principally new flying vehicles (for instance, solar sail, etc.) for reaching the velocity required for leaving the Solar system, will be a prerequisite for a successful exploration of the planets in other galaxies.

The progress made by mankind in space exploration is certainly great, and the pace of development of various areas of space technology will only be increasing in the future, thus confirming its revolutionary impact. Commercialization which has become very explicit recently, this leading to narrowing of the research programs, certainly raises concern. One still can be sure, however, that through the efforts of international cooperation in the space area, it will be possible to implement more than one grandiose project on study of the fundamental space phenomena, construction of industrial facilities in the terrestrial orbit, of lunar outposts, making flights to other planets and that the world experience of space technology gained over the past years, will be used in all these developments.

WELDABILITY OF HIGH-STRENGTH ALLOYS OF Al–Zn–Mg–(Cu) SYSTEM (Review)

A.Ya. ISHCHENKO and **V.O.CHAPOR**
The E.O. Paton Electric Welding Institute, NASU, Kyiv, Ukraine

ABSTRACT

The problems of welding high-strength alloys of Al–Zn–Mg–(Cu) system are considered. The effect of chemical composition of alloys and filler material on the weldability characteristics is analyzed. Causes of defect formation in the welded joint are described. The problems of weldability and degree of metal weakening under the action of a thermal cycle depending on the method of welding are outlined. The further investigations for improving weldability of alloys of Al–Zn–Mg and Al–Zn–Mg–(Cu) systems are predicted.

Key words: *welding, heat treatment, aluminium alloys, zinc, magnesium, copper, scandium, weldability, welded joints, strength, toughness, hot cracks, porosity, corrosion cracking, service properties.*

In modern industry the aluminium high-strength alloys which are characterized by a low specific density and good corrosion resistance are widely used for manufacture of welded structures. In spite of using good-weldable aluminium alloys of such systems of alloying as Al–Mg (AMg6, 1570), Al–Mg–Si (AD31, AD33, AD35, 6013), Al–Cu–Mn (1201), the alloys of system Al–Zn–Mg–(Cu) attract continuously the interest of the designers and researchers [1 – 6].

The alloys of Al–Zn–Mg system are featured by a preserving of oversaturated solid solution at comparatively low rates of air cooling from high temperatures (self-quenching) and by the ability to be hardened in the process of a natural ageing. Due to this the welded joints have a high strength without a repeated quenching, as the air cooling after welding is quite sufficient to produce an oversaturated solid solution in weld metal and HAZ, and, consequently, the hardening at the expense of a next natural ageing [7 – 10].

In addition, alloys of Al–Zn–Mg system are characterized by a high adaptability to manufacture, in particular a high deformability at plastic metal working. The outflow rate in pressing is only inferior to that of alloys Al–Mg–Si (AD31) and much higher than that of alloys of system Al–Cu–Mg (D16) and Al–Mg (AMg6, 1570), especially in alloys with a lithium, characterized by a complex technology of production [11 – 15].

Alloys of system Al–Zn–Mg–Cu are most high-strength [8, 11, 16, 17]. The mean ultimate rupture strength after artificial ageing is about 650 MPa, and the increase in a total percent of alloying (10 % Zn, 4.0 – 4.5 % Mg, 1.5 – 2.0 % Cu) can provide the strength level above 800 MPa. They are subjected to the plastic metal working under the conventional conditions and some of them can be deformed under the conditions of superplasticity that makes them attractive from the technological point of view for manufacture of sheet and other prefabrications [18].

The negative characteristic of the alloys, alloyed with zinc and magnesium, is an increased susceptibility to the corrosion cracking and stress corrosion. It is most clearly expressed in case of the material ageing for a maximum strength, i.e. in reaching the condition T1 (Russia) or T6 (USA) [5, 8, 17, 19, 20]. In this connection, the alloys as a rule are used in an overaged condition, in which they are characterized by a good corrosion resistance in combination with mean values of strength characteristics.

Taking into account these peculiarities of alloys of the mentioned system of alloying the following alloys, which contain a small total amount of zinc and magnesium (5 – 7 %), found a wide application for welded structures: 1911, V92Ts, 1915 (Russia); 7039, 7005 (USA); AlZnMg1 (Germany); AZ5G (France); GA6950 (Sweden); A7NO1 (Japan) (Table 1). In addition, their susceptibility to the intercrystalline corrosion is at the level of this parameter of alloys of Al–Mg system. It is considered that at this total content of zinc and magnesium within the ranges from 5.5 to 6.5 % the alloys of the mentioned system are characterized by a low susceptibility to the stress corrosion cracking. Optimum zinc-to-magnesium ratio which provides the mentioned properties is approximately 0.8 [7, 15, 21, 22]. Strength characteristics of alloys of system Al–Zn–Mg are given in Table 2.

Addition of 2 – 3 % of copper improves remarkably the corrosion properties of alloys of Al–Zn–Mg system. However, in this case the sensitivity to the rate of cooling in quenching is increased signifi-

Table 1. Chemical composition of alloys of Al–Zn–Mg system, %

Alloy grade	*Country*	*Zn*	*Mg*	*Mn*	*Cr*	*Zr*	*Ti*	*Cu*	*Fe*	*Si*
7046	USA	6.6 – 7.6	1.00 – 1.60	≤ 0.3	≤ 0.2	0.10 – 0.18	–	≤ 0.25	≤ 0.40	≤ 0.20
7039		3.5 – 4.5	2.30 – 3.30	0.1 – 0.4	0.15 – 0.25	–	≤ 0.10	≤ 0.10	≤ 0.40	≤ 0.30
7005		4.0 – 4.5	1.00 – 1.80	0.2 – 0.7	0.06 – 0.20	0.08 – 0.20	–	≤ 0.10	≤ 0.40	≤ 0.35
1911	Russia	3.8 – 4.4	1.60 – 2.10	0.2 – 0.5	0.07 – 0.25	0.13 – 0.22	–	0,10 – 0.20	≤0 .30	≤ 0.20
1915		3.4 – 4.0	1.30 – 1.80	0.2 – 0.6	0.08 – 0.20	0.10 – 0.20	≤ 0.10	≤ 0.10	≤ 0.40	≤ 0.30
V92Ts		2.9 – 3.6	3.90 – 4.60	0.6 – 1.0	–	0.06 – 0.20	0.01 – 0.66	≤ 0.50	≤ 0.35	≤ 0.35
AlZnMg1	Germany	4.0 – 5.0	1.00 – 1.40	0.1 – 0.5	0.10 – 0.25	–	0.01 – 0.20	≤ 0.10	≤ 0.50	≤ 0.50
AZ5G	France	4.1 – 4.9	0.90 – 1.40	≤ 0.3	0.15 – 0.35	0.05 – 0.25	0.01 – 0.20	≤ 0.10	≤ 0.40	≤ 0.30
ZK60	Japan	6.0	0.75	0.2	–	0.16	–	≤ 0.10	≤ 0.30	≤ 0.20
A7NO1		4.5	1.40	0.4	0.10	0.15	–	–	–	–
GA6950	Sweden	4.8	1.10	0.25	0.20	–	≤ 0.20	–	–	–

cantly, i.e. the effect of «self-quenching» is eliminated.

The level of strength of traditionally weldable alloys of Al–Zn–Mg system does not exceed 500 MPa, here σ_t^W is approximately 400 MPa. Susceptibility to hot cracking in fusion welding is mainly suppressed by additions of titanium, zirconium and cerium.

Some works on investigation of weldability of alloys of this system were devoted to the study of effect of welding stresses on the fracture resistance of joints. It is stated that limitation of the period of time between welding and beginning of the artificial ageing of welded joints up to two days can preserve the value of a specific energy of propagation of cracks the same as in the parent metal [23, 24, 8]. In addition, use of such technological processes as the removal of burn-throughs, metal thickening for welding increases significantly the level of safe stresses [25].

Welded structures from alloys of Al–Zn–Mg system are used mainly without postweld heat treatment. Moreover, welded joints, owing to the effect of «self-quenching» and subsequent natural ageing possess high enough characteristics of strength and toughness, but their total corrosion resistance is low. The use of a repeated artificial

Table 2. Mechanical properties of alloys of Al–Zn–Mg system at room temperature

Alloy grade (condition)	*Kind of prefabrication*	σ_t, *MPa*	$\sigma_{0.2}$, *MPa*	δ, *%*
1911 (T2)	Rolled	430	360	11.0
1911 (T2)	Pressed	450	400	10.0
1915 (T1)	Rolled	350	300	10.0
1915 (T1)	Pressed	435	383	14.2
V92Ts (T1)	Rolled	400	300	10.0
V92Ts (T1)	Pressed	450	350	10.0
7005 (T53)	»	392	345	15.0
7005 (T6)	Rolled	324	262	10.0
7039 (T64)	Pressed	450	380	13.0
ZK60	»	360	320	12.0

ageing after welding can increase the structure resistance to corrosion, but the welded joints become more susceptible to a delayed fracture. The ageing of a finished welded structure causes difficulties in the manufacturing technology.

In works devoted to the study of weldability of alloys of Al–Zn–Mg–Cu system (V95, V96Ts (Russia); ESD (Japan); A-Z8GV (France); Z74S (Germany); DTD 5150 (UK); 7178, 7475, 7075, 7175 (USA) showed that during welding these alloys are characterized by a high sensitivity to the formation of hot cracks and also possess unsatisfactory toughness of the welded joints. Therefore, the high-strength alloys did not find wide application in the welded structures. The absence of optimized conditions of heat-treatment which could provide high strength and toughness and a good resistance to the stress corrosion cracking made their application in industry much less common. As a result, during long time in aerospace and other industries the traditional medium-strength alloys were used [26 – 29].

Over the recent time the investigations of alloys of Al–Zn–Mg–(Cu) system were continued to improve their strength characteristics, to increase the resistance to the stress corrosion at high characteristics of weldability.

Comprehensive investigations were made on alloying using transition and rare-earth metals. One of the most important results of these works was the development of compositions of industrial alloys additionally alloyed with scandium additions, for example, alloys of grades 1970 (Al–5.2 Zn–2.0 Mg–0.4 Cu–0.2 Sc–0.1 Zr) and 1975 (Al–5.2 Zn–2.0 Mg–0.3 Cu–0.07 Sc–0.1 Zr).

Ultimate rupture strength of alloy of the 1970 grade reaches 470 MPa, yield strength 410 MPa for plates, while for sheets they are 560 and 521 MPa, respectively. Additions of ≥0.2 % scandium provide high characteristics of strength, make alloy superplastic and improve the adaptability to manufacture of sheet and other prefabrications made of them. In addition, the tests showed that alloys are characterized by a very low degree of

Table 3. Chemical composition of alloys of system Al–Zn–Mg–Cu, %

Alloy grade	*Country*	*Zn*	*Mg*	*Cu*	*Mn*	*Cr*	*Zr*	*Ti*	*Fe*	*Si*
7075	USA	5.1 – 6.1	2.1 – 2.9	1.2 – 2.0	≤ 0.30	0.18 – 0.24	–	≤ 0.20	≤ 0.50	≤ 0.40
7475		5.2 – 6.2	1.9 – 2.6	1.2 – 1.9	≤ 0.06	0.18 – 0.25	–	≤ 0.06	≤ 0.12	≤ 0.10
7050		5.7 – 6.7	1.9 – 2.6	2.0 – 2.6	≤ 0.10	≤ 0.04	0.08 – 0.15	≤ 0.06	≤ 0.15	≤ 0.12
7150		5.9 – 6.9	2.0 – 2.7	1.9 – 2.5	≤ 0.10	≤ 0.04	0.80 – 0.15	≤ 0.06	≤ 0.15	≤ 0.12
7178		6.3 – 7.3	2.4 – 3.1	1.6 – 2.4	≤ 0.30	0.18 – 0.28	–	≤ 0.20	≤ 0.50	≤ 0.40
7055		7.6	1.8 – 2.3	2.0 – 2.6	≤ 0.05	≤ 0.04	0.05 – 0.25	≤ 0.06	≤ 0.15	≤ 0.10
V95	Russia	5.0 – 7.0	1.8 – 2.8	1.4 – 2.0	0.20 – 0.60	0.10 – 0.25	–	–	≤ 0.50	≤ 0.50
1963		6.0 – 7.0	2.5 – 3.1	1.6 – 2.0	–	0.14 – 0.18	0.12 – 0.18	–	≤ 0.30	≤ 0.15
V96		7.6 – 8.9	2.5 – 3.2	2.2 – 2.8	0.20 – 0.50	0.10 – 0.25	–	–	≤ 0.50	≤ 0.30
V96Ts		8.0 – 9.0	2.3 – 3.0	2.0 – 2.6	0.10	0.10	0.10 – 0.20	–	≤ 0.40	≤ 0.30

anisotropy of properties and high characteristics of crack resistance. Effectiveness of scandium use in alloys of Al–Zn–Mg system is explained by the fact that none of main alloying elements forms intermetallic compounds with it [30, 31].

To improve the properties, it is recommended to alloy the alloys with combined additions of scandium and zirconium. This saves an expensive scandium and intensifies greatly its positive action [30, 32].

Welded joints of alloy of grades 1970 and 1975 without a special heat treatment (three months of postweld natural ageing) have 450 MPA ultimate rupture strength. The safe level of stresses of welded joints characterizing the resistance to stress corrosion to a delayed fracture is rather high, i.e. 225 and 200 N/mm^2, respectively [30].

At present the alloys of Al–Zn–Mg–Sc system are most high-strength and possess a good weldability. It is evident that this alloying with rare-earth metals will become one of the most promising trends in the development of high-strength alloys of series 7XXX with good strength, service characteristics and weldability.

In references [33 – 35] there is information about the positive effect of small additions of lanthanum on the mechanical properties of alloys of Al–Zn–Mg–Cu system. In addition, it is noted that it can decrease the susceptibility of alloys to cracking.

The investigations carried out on alloying with small additions of silver showed that in this case the resistance to stress corrosion is increased, but the weldability is noticeably deteriorated [15, 36]. However, the latter circumstance did not prevent the Japanese researchers to develop a group of high-strength alloys containing additions of silver. Chemical composition of these alloys is as follows, %: 5 – 8 Zn; 1.2 – 4.0 Mg; 1.5 – 4.0 Cu; 0.03 – 1.00 Ag; 0.01 – 1.00 Fe; 0.005 – 0.200 Ti; 0.01 – 0.20 V. It also includes one of the following elements, %: 0.01 – 1.50 Mn; 0.01 – 0.60 Cr; 0.01 – 0.25 Zr; 0.0001 – 0.0800 B; 0.03 – 0.50 Mo or combination of several mentioned elements. Here, it is also noted that these alloys are differed from others by a high level of resistance to stress corrosion cracking [37, 38].

A remarkable progress in the development and application of high-strength alloys of Al–Zn–Mg–(Cu) during recent decades is due to the research works directed to the development of special conditions of heat treatment (to improve the corrosion resistance at high level of strength characteristics). As a result of these works, a phenomenon of a retrogression, known for aluminium alloys since the 1930s, began to be used in the conditions of heat treatment of prefabrications. Conditions RRA (Retrogression and Reageing), known as T77, include heat treatment for a maximum strength (quenching + artificial ageing), retrogression and reageing for a maximum strength. As a result, the products of alloys of 7075 grade reach maximum strength and high characteristic of resistance to corrosion cracking and layer corrosion both in condition T1 (Russia) and condition T3 (Russia) [39 – 49].

This resulted in the feasibility of application of high-strength alloys in structures of new aircrafts, etc. [50, 51]. The use of plates from alloys of grades 7150 (T7751) and 7055 (T7751) in the design of aircraft «Boeing-777» could reduce its mass for 1450 kg. Chemical composition and main mechanical properties of alloys of system Al–Zn–Mg–Cu, used in industry [52, 53], are given in Tables 3 and 4.

Welded structures of alloys of Al–Zn–Mg–Cu system are used after repeated artificial ageing that can increase their ultimate rupture strength to 0.8 σ_t of the parent metal.

There are no data in references about the weldability of these alloys treated by the condition T77. It is evident that examination of their weldability in this condition or with a subsequent heat treatment of welded joints including RRA is a challenging trend [54, 55].

The study of parameters of weldability of alloys of grade 1963 (Al–6 – 7 Zn–2.5 – 3.1 Mg–1.6 – 2.0 Cu–0.14 – 0.18 Cr–0.12 – 0.18 Zr, < 0.3 Fe,

Table 4. Mechanical properties of alloys of system Al–Zn–Mg–Cu at room temperature

Alloy grade (condition)	*Type of prefabrication*	σ_t, *MPa*	$\sigma_{0.2}$, *MPa*	δ, *%*
V95 (T1)	Rolled	530	480	11
V95 (T1)	Pressed	580	550	8
V95 (T2)	»	550	500	10
V96Ts (T1)	»	650	630	6
7050 (T73)	Plate	510	455	11
7075(T6)	Rolled	538	470	8
7178 (T6)	Pressed	605	540	11
7475 (T6)	Rolled	552	496	12

< 0.15 Si), etc., showed that the optimum filler for alloys of series 7XXX is the wire from alloys of Al–Mg system. Sensitivity to cracking in welding with wire Sv-AMg6 is twice lower than that in welding with wire close in composition to the parent material (Al–Zn–Mg–Cu). Here, the toughness of welded joints made with Al–Mg wire two times exceeds the toughness of joints welded with wire of Al–Zn–Mg–Cu system [18, 56, 57].

According to results of investigations [18], the most effective filler in welding alloys of 1963 grade in comparison with wire Sv-AMg6 is the material of alloy of 1557 grade. For welding alloys of grades 7072, 7075, A7N01 with a consumable electrode, the wire which contains an increased amount of magnesium (to 9 %) using additions of zinc, titanium, manganese, chromium as modifiers, was suggested. Increase in magnesium content in weld metal promotes the decrease in susceptibility to hot cracking. Here, the presence of manganese and chromium reduces effectively the susceptibility to stress corrosion cracking [58 – 61]. Strength of welded joints is at the level of 0.7 σ_t of the parent metal.

Research works, carried out at the PWI, confirmed the rationality of using new filler materials on Al–Mg base in welding alloys of series 7XXX. Addition of scandium to the weld metal in welding alloys of Al–Zn–Mg system reduces significantly the susceptibility to hot cracking, increases the strength characteristics of welded joints. In welding alloys, which contain 2 – 3 % copper, the addition of scandium is less effective.

There is still no a single opinion concerning the effect of scandium on characteristics of weldability of copper-containing alloys. From the one hand, the addition of scandium into the alloy of grade 1933 (Al–6.8 Zn–1.9 Mg–1.0 Cu–0.2 Sc–0.1 Zr) contributes to the increase in strength characteristics, the decrease in anisotropy of properties and sensitivity to cracking [33]. The works of other researchers state that the alloying of aluminium copper-containing alloys with scandium does not always lead to the refining of crystalline structure of the weld metals and to the improvement of their strength characteristics. This is explained by that the scandium and copper can form a chemical compound, such *W*-phase ($ScCu_{6.6-4.0}$; $Al_{5.4-8.0}$). In this case scandium does not participate in the alloy hardening and refining of its structure, and the increase in a volume fraction of an excessive phases leads to the reduction in strength, toughness and fracture toughness [62]. Therefore, the further works are necessary to determine the rationality of alloying the alloys of Al–Zn–Mg–Cu system with the scandium.

The study of effectiveness of different methods of fusion welding showed that the electron beam welding provides higher strength by 15 – 20 % than the argon-arc welding. In alloys with a total amount of zinc and magnesium of about 8 % after ageing, it amounts to 0.86 % of that of the parent metal [63]. The improvement of strength characteristics, the reduction of defect quantity in welded joints during electron beam welding is provided at the expense of a high specific concentration of energy, favourable conditions of a vacuum protection of the molten metal, low value of heat input (4 – 5 times lower than in argon-arc welding), small HAZ, small volume of the weld pool metal [64 – 68]. In addition, double-sided (from the side of beam and penetration) evolution of gases and vapours of metal from the penetration channel decreases the amount of pores and cavities in the weld metal [69].

From data of [23, 70, 71] the application of plasma-arc method for welding alloys of 1963 grade was recognized unsuitable. However, the arguments stated are not convincing, as the energy concentration in plasma-arc is much higher than in argon-arc welding that contributes to the decrease in heat input of welding and influence favourably the HAZ metal. Probably, the further more profound investigations of this method of fusion welding are required, as this method was also well-suitable for welding other alloys related to series 7XXX.

The improvement of properties of welded joints in argon arc welding with a non-consumable electrode is attained due to using a pulsed arc, by decreasing a heat input, formation of fine-crystalline structure and decrease in amount of oxide films in weld metal. The application of a pulsed current in welding with consumable electrode stabilizes the electrode metal transfer. Replacement of argon by helium or use of mixture Ar + He can greatly decrease the volume of voids in the weld metal [45, 72].

It was established from the analysis, that the application of high-purity alloys both as a parent and filler metal is an optimum condition for producing quality welded joints from the alloys of Al–Zn–Mg–(Cu) system with high strength and service characteristics. Especially, the level of saturation with hydrogen is regulated that promotes the significant improvement of the welded joint quality, and also the application of electron beam welding under strictly controlled conditions. In addition, it is necessary to take into account that zinc and magnesium influence positively the penetration of alloy (heat input is decreased), but at the same time the large losses of zinc and magnesium for evaporation are observed during welding. To avoid these losses it is recommended to perform welding at increased rates of more than 40 m/h [69, 71].

CONCLUSIONS

During welding the alloys of Al–Zn–Mg–(Cu) system are characterized by a low resistance to hot crack formation, unsatisfactory level of toughness of welded joints, the susceptibility to stress corrosion cracking. Therefore, to improve the weldability of alloys of Al–Zn–Mg–(Cu) system the following investigations seem to be promising:

optimizing the chemical composition both of parent and filler materials. The further investigation of effect of scandium, other transition and rare-earth metals on strength, service characteristics, of weldability of alloys with an increased total content of zinc and magnesium seems to be challenging;

application of effective methods of casting and post treatment, which provide favourable metallurgical heredity to improve the weldability, for producing parent and filler material;

development of conditions of heat treatment of alloys and also determination of optimum their combination with a thermal cycle of welding that could preserve high strength properties of the parent metal, increase the resistance to stress corrosion and improve the properties of the welded joints as a whole;

application of highly effective methods of welding (electron beam, argon-arc nonconsumable electrode welding with a pulsed and constricted arc, with a pulsed current in consumable electrode welding), due to which the favourable conditions for producing quality welded joints with a high safety factor are provided.

REFERENCES

1. Rabkin, D.M. (1986) *Metallurgy of fusion welding of aluminium and its alloys*. Kiev: Naukova Dumka.
2. Mondolfo, L.F. (1976) *Aluminium alloys structure and properties*. London: Boston.
3. Kolachev, B.A., Livanov, V.A., Elagin, V.I. (1981) *Metals science and heat treatment of non-ferrous metals and alloys*. Moscow: Metallurgia.
4. Elagin, B.I., Zakharov, V.V., Filatov, Yu.A. (1996) About prospects of application of new high-strength weldable alloy 01570 (Al–Mg–Sc) in aircraft industry. In: *Treatment of light and special alloys*. Moscow: Metallurgia.
5. (1972) *Aluminium. Metals science, treatment and application of aluminium alloys*. Ed. by A.T. Tumanov, F.I. Kvasov, I.N. Fridlyander. Moscow: Metallurgia.
6. Yoshida, H., Uchida, H. (1993) Recent investigations and development of aluminium alloys for aircraft industry. *Sumitomo Light Metal Techn. Rep.*, **34**, 87 – 89.
7. (1972) Aluminium alloys. In: *Weldable alloys*. Ed. by I.N. Fridlyander. Moscow: Metallurgia.
8. Mironenko, V.N., Evstifeev, B.S., Sharapov, V.V. (1981) Local heat treatment of welded joints of alloy 1911. *Svarochnoye Proisvodstvo*, **1**, 17 – 19.
9. Itoh, G., Kuramoto, S., Kano, M. (1991) Effect of copper additions on tensile properties of alloy Al–4.4 Zn–1.4 Mg. *J. Jap. Inst. Light Metals*, **3**, 184 – 191.
10. Lukasak, D.A., Hart, R.M. (1991) Aluminium alloy development efforts for compression dominated structure of aircraft. *Light Metal Age.*, **9/10**, 11 – 15.
11. Chayun, A.G., Labur, T.M., Yavorskaya, T.R. (1985) Selection of filler wire for welding high-strength aluminium-lithium alloy 1420. In: *Actual problems of welding non-ferrous metals*. Kiev: Naukova Dumka.
12. Fridlyander, I.N., Chuistov, K.V., Berezina, A.L. *et al.* (1992) *Aluminium–lithium alloys. Structure and properties*. Kiev: Naukova Dumka.
13. (1986) Aluminium–lithium alloys. In: *Proc. of the 3rd Int. Conf. on Aluminium–Lithium*, London, 1986. London: The Institute of Metals.
14. Elagin, B.I. (1994) New strengthening treatment of aluminium alloys using the retrogression. *Tekhnologia Lyogkikh Splavov*, **5/6**, 5 – 10.
15. Elagin, B.I., Zakharov, V.V., Drits, A.M. (1982) *Structure and properties of alloys of Al–Zn–Mg system*. Moscow: Metallurgia.
16. Dobatkin, V.I., Elagin, V.I., Fyodorov, V.M. (1995) *Quick-crystallized alloys*. Moscow: VILS.
17. Fridlyander, I.N., Kutaitseva, E.I. (1956) *High-strength aluminium alloy B95 (Al–Zn–Mg–Cu)*. Moscow: Metallurgia.
18. Sukhoverkhov, A.A., Postnova, A.A., Kurbatov, N.G. (1980) Effect of composition of filler wire on technological and mechanical properties of welded joints of alloy 01963. *Aviats. Materialy*, **4**, 127 – 130.
19. Elagin, B.I., Zakharov, V.V. (1994) New trend in heat treatment of aluminium alloys. *Metallovedeniye i Term. Obrabotka Metallov*, **11**, 30 – 35.
20. Polmear, I.J. (1981) Stress corrosion cracking in weldable Al–Zn–Mg alloys. *Corros. Austral.*, **4**, 4 – 9.
21. Nikolaev, G.A., Fridlyander, I.N., Arbuzov, Yu.P. (1990) *Weldable aluminium alloys*. Moscow: Metallurgia.
22. Sinyavsky, V. S., Valkov, V.D., Budov, G.M. (1979) *Corrosion and protection of aluminium alloys system*. Moscow: Metallurgia.
23. Sukhoverkhov, A.A. (1995) Towards the problems of weldability of alloys of Al–Zn–Mg–Cu system. *Svarochnoye Proizvodstvo*, **7**, 11 – 15.
24. Zenkova, E.K., Kramotin, V.N., Maltsev, M.V. (1970) Kinetics of crack propagation in alloy ATsM at delayed fracture. *Fiziko-khimicheskaya Mekhanika Materialov*, **1**, 30 – 34.
25. Zaitseva, N.I., Artyomova, M.S., Kadobnova, N.V. *et al.* (1980) Resistance to delayed fracture of welded joints of alloy of Al–Zn–Mg system. *Aviats. Materialy*, **4**, 116 – 120.
26. Kramer, L.S., Tack, W.T., Fernandes, M.T. (1997) Modification on aluminium alloys via scandium additions. In: *Proc. ALUMITECH'97*, Atlanta, 1997. Atlanta.
27. Blewett, R.V. (1981) Aluminium alloys for structural use. *FWP J.*, **1**, 73 – 82.
28. Ohnishi, T., Yoshimura, K. (1987) Corrosion fatigue of aluminium alloy 7075. *J. Jap. Inst. Light Metals*, **2**, 127 – 133.
29. Hunt, M. (1990) Aerospace aluminium. *Mater. Eng.*, **8**, 27 – 30.
30. Davydov, V.G., Elagin, B.I., Zakharov, V.V. *et al.* (1996) About alloying of aluminium alloys with additions of scandium and zirconium. *Metallovedeniye i Term. Obrabotka Metallov*, **8**, 25 – 30.
31. Khan, G.M., Nikiforov, A.O., Zakharov, V.V. *et al.* (1993) Effect of scandium content on structure and characteristics of superplasticity of aluminium alloys of Al–Zn–Mg–Sc–Zr system. *Tsvetnyye Metally*, **11**, 55 – 58.

32. Toropova, L.S., Dobatkina, T.V., Kamardinkin, A.N. (1992) Polythermal section of Al–Sc–Zr system. *Metally*, **5**, 140 – 143.
33. Kishi, Y., Hirose, Y., Tsukuda, I. (1994) Effect of Cr, Mn, Mg content on characteristics of strength and stress corrosion cracking of extruded alloys of Al–Zn–Mg–Cu–La system. *J. Soc. Mater. Sci.*, **485**, 210 – 216.
34. Kishi, Y., Hirose, Y., Tsukuda, I. *et al.* (1994) Effect of Zr addition on microstructure and mechanical properties of extruded alloys of Al–Zn–Mg–La system with a high resistance to stress corrosion cracking. *Ibid.*, **492**, 1113 – 1119.
35. Kishi, Y., Tsukuda, I., Higashi, K. *et al.* (1994) The mechanical properties and SCC life of extruded Al–Zn–Mg–Cu–La system alloys improved by Cr, Mn, Mg addition. In: *Proc. of 4th Int. Conf. on Offshore and Polar Eng.*, Osaka, 1994. Colorado: Golden.
36. Polmear, I.J. (1989) Development of high-strength aluminium alloys containing minor additions of silver. In: *Austral. aeron. conf. on Res. and Technol.*, Melbourne, 1989. Melbourn: Barton.
37. Tomiharu, O., Takeru, M., Kazuyoshi, K. *et al. Weldable high-strength aluminium alloy with a high resistance to the stress corrosion cracking*. Pat. **4-13829** Japan, Int. Cl. C 22 C 21/10. Publ. 17.01.92.
38. Tomiharu, O., Takeru, M., Kazuyoshi, K. *et al. Weldable high-strength aluminium alloy with a high resistance to the stress corrosion cracking*. Pat. **4-13832** Japan, Int. Cl. C 22 C 21/10. Publ. 17.01.92.
39. Chuichi, O., Shigeyuki, K. *Heat treatment of aluminium alloys of 7000 type*. Pat. **62-142753** Japan, Int. Cl. C 22 F 1.053, C 22 C 21/10. Publ. 25.06.87.
40. Park, J.K. (1988) Influence of retrogression and reageing treatments on the strength and stress resistance of aluminium alloy 7075-T6. *Mater. Sci. and Eng.*, **3**, 223 – 231.
41. Ohnishi, T., Ibaraki, Y., Itoh, T. (1988) Improvement of fracture toughness of aluminium alloy 7475 by RRA process (retrogression and reageing). *J. Jap. Inst. Metals*, **9**, 872 – 877.
42. Ohnishi, T., Ibaraki, Y., Itoh, T. (1989) Improvement of fracture toughness in 7475 aluminium alloy by the RRA (retrogression and reageing) process. *Mater. Trans. JIM*, **8**, 601 – 607.
43. Hashmi, F.H., Khan, A.Q. (1989) Creep properties of 7075 aluminium alloy under intermittent stressing. *Pakistan J. Sci. and Ind. Res.*, **32**, 141 – 144.
44. Pyun, S.-I,, Choi J.-K. (1989) Some indices characterizing susceptibility to stress-corrosion cracking of Al–Zn–Mg–Cu alloy. *J. Mater. Sci. Lett.*, **12**, 1402 – 1404.
45. Rabkin, D.M., Dovbyshchenko, I.V., Dykhno, V.M. *et al.* (1989) Thermal state of electrode drops and porosity in welding aluminium and its alloys. In: *Welding of non-ferrous metals*. Kiev: Naukova Dumka.
46. Ohnishi, T., Itoh, T. (1989) Effect of retrogression and reageing treatments on stress corrosion cracking and fracture toughness of Al–Zn–Mg–Cu alloy. In: *Proc. of 8th Int. Conf. on Strength of Metals and Alloys*, Tampere, 1988. Oxford.
47. Brown, M.H., Staley, J.T., Liu, J. *et al. Aluminium alloy product having improved combination of strength and corrosion resistance properties and method of producing the same*. Pat. **4863528** USA, Int. Cl. C 22 F 1/04. Publ. 10.09.90.
48. Krivov, V.A., Ryabov, V.R., Ishchenko, A.Ya. *et al.* (1998) *Welding in aircraft industry*. Kiev: MIIBTs.
49. Alarcon, O.E., Nazar, A.M., Monteiro, W.A. (1991) The effect of microstructure on mechanical behaviour and fracture mechanism in a 7050-T76 aluminium alloy. *Mater. Sci. and Eng.*, **2**, 275 – 285.
50. Orman, L., Klyszewski, A. (1991) Effectiveness estimation of heat treatment practice of Al–Zn–Mg–Cu (7075) aluminium alloy as measured in hot compression test. *Arch. Met.*, **4**, 387 – 393.
51. Srivatsan, T.S. (1992) Microstructure, tensile properties and fracture behaviour of aluminium alloy 7150. *J. Mater. Sci.*, **17**, 4772 – 4781.
52. Dorey, G., Peel, C.J., Curtis, P.T. (1994) Advanced materials for aerospace structures. *Proc. Inst. Mech. Eng.*, **1**, 1 – 8.
53. (1995) New aluminium alloys in Boeings's 777. *Metal Bull.*, **8**, 65.
54. Masao, K., Takeo, V., Masao, M. (1981) Characteristics of HAZ of welded joints of Al–Zn–Mg alloy after two-stage ageing. *J. Jap. Inst. Light Metals*, **3**, 151 – 156.
55. Fyodorova, L.V., Osintsev, O.E., Fyodorov, V.M. (1995) Design strength and weldability of alloy 01949. In: *New materials and technologies*. Abstr. of pap. Moscow.
56. Dorn, L., Jahn, P., Doerk, P. (1981) Pulsed-arc welding of Al-4.5 Zn-1 Mg aluminium alloy. *Schweiss. und Schneid.*, **12**, 224 – 225.
57. Masatoshi, E., Shigetoshi, S. *Combined filler material of aluminium*. Pat. **3-169495** Japan, Int. Cl. B 23 K 35/02. Publ. 10.09.91.
58. Arai, K., Otsuka, Y., Tsukamoto, K. *et al. Filler metal for welding alloys Al–Zn–Mg*. Pat. **56-77358** Japan, Int. Cl. C 22 C 21/06, B 23 K 35/28. Publ. 25.06.81.
59. Beier, R. (1982) Welding of alloys on Al–Zn–Mg base. *Anlag. + Verfahr.*, **4**, 78, 81 – 82, 84.
60. Reznichenko, B.M., Nikitin, V.M. (1994) Effect of chemical composition of weld on mechanical properties of welded joints of alloy of Al–Zn–Mg system. In: *New materials and technologies.* Abstr. of pap. Moscow.
61. (1992) ALCOTEC filler metal 5180 (Al–Zn–Mg alloy family weld wire). *Alloy Dig.*, **9**, 3 – 4.
62. Zakharov, V.V., Rostova, T.D (1995) Alloying of aluminium copper-containing alloys with scandium. *Metallovedeniye i Term. Obrabotka Metallov*, **2**, 23 – 27.
63. Reznichenko, B.M. (1994) Effect of heat treatment on properties of welded joints of alloy of Al–Zn–Mg system. In: *New materials and technologies*. Abstr. of pap. Moscow.
64. Bondarev, A.A., Rabkin, D.M. (1974) Evaporation of easily-volatile elements in electron beam welding of aluminium alloys. *Avtomaticheskaya Svarka*, **3**, 13 – 16.
65. Bondarev, A.A., Voropay, N.M., Ishchenko, A.Ya. *et al.* (1972) Effect of technological factors of porosity of aluminium welds made by electron beam welding. *Ibid.*, **8**, 24 – 26.
66. Sharkov, A.N., Klykov, N.A., Bondarev, A.A. *et al.* (1978) Electron beam welding of aluminium alloy B93. *Svarochnoye Proizvodstvo*, **5**, 17 – 18.
67. Bondarev, A.A. (1990) Investigation of weldability of high-strength alloy of Al–Zn–Mg system by using EBW. *Avtomaticheskaya Svarka*, **9**, 36 – 38.
68. Bondarev, A.A. (1984) State-of-the-art of equipment and advantages of process of electron beam welding structures of aluminium alloys. In: *Welding of aluminium alloys of cryogenic and general purpose*. Kiev: Naukova Dumka.
69. Alov, A.A. (1978) Effect of heredity on weldability of deformed prefabrications of aluminium alloys. *Avtomaticheskaya Svarka*, **6**, 37 – 39.
70. Elagin, B.I., Zakharov, V.V., Rostova, T.D (1994) Effect of scandium on structure and properties of alloy Al–5.5 Zn–2.0 Mg. *Metallovedeniye i Term. Obrabotka Metallov*, **7**, 1 – 5.
71. Talaev, V.S., Sukhoverkhov, A.A., Danilkin, V.A. (1979) Hydrogen distribution in welded joints of alloy of Al–Zn–Mg–Cu system. *Svarochnoye Proizvodstvo*, **9**, 7 – 9.
72. Ishchenko, A.Ya., Dovbyshchenko, I.V., Budnik, V.P. *et al.* (1994) Advanced methods of welding aluminium alloys. *Avtomaticheskaya Svarka*, **5/6**, 35 – 37.

CONTROL OF BEAD FORMATION IN ARC SURFACING WITH STRIP ELECTRODE

A.D. RAZMYSHLYAEV
Priazov State Technical University, Mariupol, Ukraine

ABSTRACT

Electromagnetic nature of a defect in the weld bead in the form of a cavity (saddle) formed in its central portion in DC submerged-arc surfacing using strip electrode is described. It is suggested that the controlling magnetic fields should be used to compensate for asymmetry of the magnetic field induced in the arc zone by the surfacing current flowing through the strip electrode extension.

Key words: arc surfacing, strip electrode, deposited bead, metal formation, electromagnetic forces.

By the data of our researchers and of study [1], in submerged-arc surfacing with strip electrode at direct current using glass-type AN-348A flux, the bead has a depression (saddle) in the center, if the surfacing current value does not exceed 400 to 500 A. An assumption can be made that the saddle forms because of higher pressure on the metal of molten slag and the flux above this slag. However, the bead saddle forms also in submerged-arc surfacing with pumice-like fluxes AN-60, OSTs-45 which have a bulk mass two times smaller than that of AN-348A flux and approximately the same thermo-physical properties of the liquid slag (in particular, also the surface tension on the liquid metal–liquid slag interface).

In surfacing with all the above fluxes at the current of about 700 A (and higher) the bead takes a convex shape. This leads to the assumption that the bead formation is affected not only by the flux properties, but also by the electromagnetic phenomena inherent to the process of surfacing with a strip electrode.

This paper gives the results of a study to establish the electromagnetic nature of saddle-like defect formation in surfacing with a strip electrode and to develop devices for their elimination.

In physical simulation of the process of surfacing with strip electrode made by the procedure of [2], no noticeable movement of the molten metal is found in the weld pool at up to 400 A surfacing current. This was the prerequisite for a more detailed analysis of the weld pool processes in the zone in which the welding arc is moving and in which the current density and the induction of the magnetic field generated as a result of the current flowing in the strip electrode stick-out, are maximal [3].

If the system of co-ordinates in Figure 1, *a* (B_s is strip width, H_s is strip stick-out) is assumed, then, as shown in [3], the tangential component of magnetic field induction B_x in the zone of the local current pick-off from the melting tip of the strip stick-out (arc) changes its sign. With the same distance from the arc axis to the left and to the right, for instance, Δy = 4 mm, the absolute value

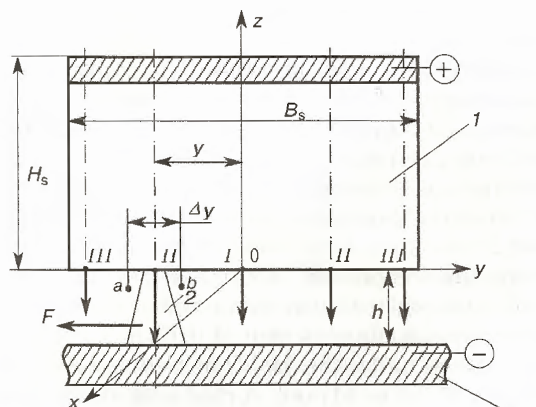

a

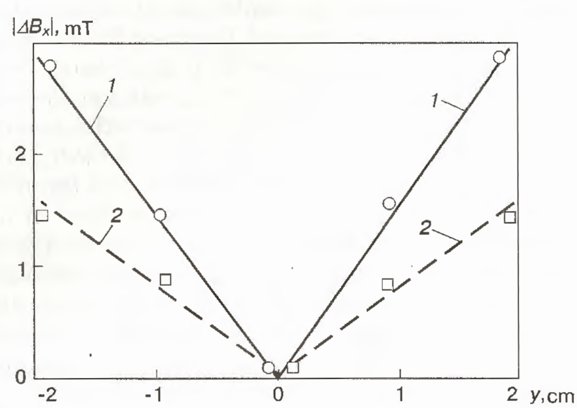

b

Figure 1. Calculated diagram of electrode stick-out (*a*) and dependence of inductance gradient on the arc location at the strip tip (*b*): *a* — *1* – electrode strip; *2* – arc; *3* – item; *I–III* – zones of arc current removal; *b* — *1* – Δ_y = 4; 2 – 8 mm.

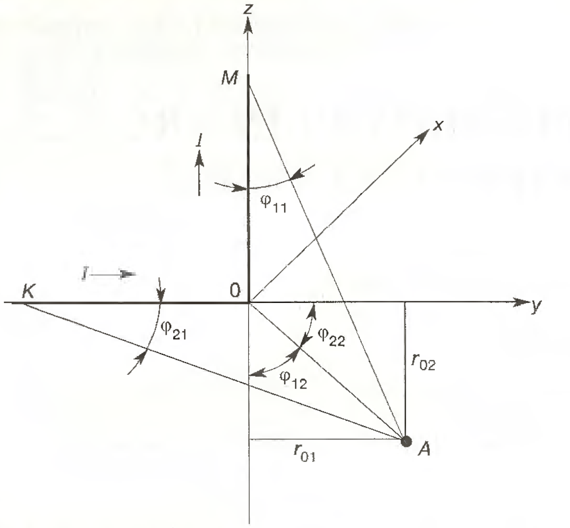

Figure 2. Diagram for calculation of magnetic field induction.

of the gradient of induction component $|\Delta B_x|$ depends on the arc position on the strip tip (arc distance y from strip axis). With the arc displacement to strip edge relative to its axis 0_z, $|\Delta B_x|$ value grows linearly. Assuming $\Delta y = 8$ mm, $|\Delta B_x|$ will become smaller, but the nature of its dependence on the position of the arc on the strip tip will remain the same (Figure 1, *b*).

With the arc displacement over the tip towards the strip edge relative to its longitudinal axis 0_z (Figure 1, *a*) a growing resultant electromagnetic force F proportional to $|\Delta B_x|$ starts acting on the arc in the same direction, i.e. the arc is accelerated [4]. Under the impact of this force, the arc is maintained at the strip edge. Interaction of $|\Delta B_x|$ with the vertical component of current density in the liquid metal under the arc gives rise to the Lorentz electromagnetic force which shifts the metal volumes located under the arc, from the center to the side edges of the weld pool. A characteristic feature of the process of surfacing with strip electrode is the fact that under the conditions of rapid solidification the side sections of the pool form a bead of greater thickness than in its central part, i.e. a saddle-type defect. The use of controlling magnetic fields can be recommended to eliminate this defect, they levelling the gradient of induction $|\Delta B_x|$ created by surfacing current flowing through the strip stick-put, and thus eliminating the gradient of induction $|\Delta B_x|$ both in the strip zone and in the liquid metal bulk under the arc. This should also eliminate the accelerated movement of the arc towards the strip electrode edges, which is achieved, if conductors through which the surfacing current flows, are placed at the strip electrode stick-out.

It is known that in point A the component of induction of the magnetic field generated in flowing of current of value I through conductors of length $0M$ and $K0$ (Figure 2), is calculated by the following formula:

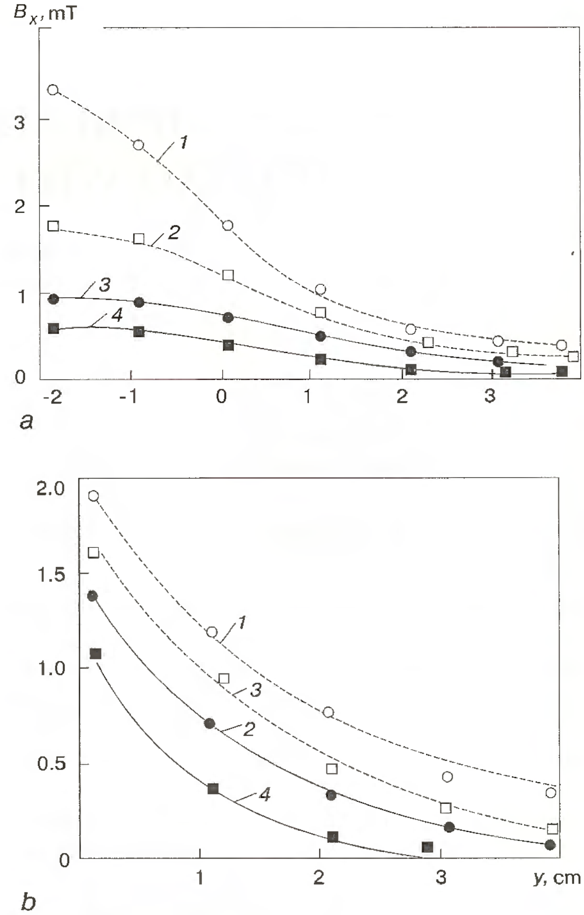

Figure 3. Distribution of the component of magnetic field induction along axis 0_y: *a* — *1* — $z = -10$ mm; *2* — -20 mm; *3* — -30 mm; *4* — -40 mm; *b* — *1*, *2* — $z = -10$ mm; *3*, *4* — -15 mm; *2*, *4* — presence of an item of a ferromagnetic material.

$$B_x = \frac{\mu_0 \mu}{4\pi} I \left(\frac{\cos \varphi_{11} - \cos \varphi_{12}}{r_{01}} + \frac{\cos \varphi_{21} - \cos \varphi_{22}}{r_{02}} \right),$$

where μ is the magnetic permeability of the environment, $\mu = 1$; μ_0 is the magnetic constant, $\mu_0 = 4\pi \cdot 10^{-7}$ H/m; r_{01}, r_{02} is the distance from the axes of conductors $0M$ and $K0$ to point A, m, respectively, and φ_{11}, φ_{12}, φ_{21}, φ_{22}, are angles.

Calculations showed that B_x in point A (its vector is normal to the plane of the drawing, see Figure 2) induced by flowing current I in conductors $K0$ and $0M$, practically does not depend on their length, if $K0 = 0M \geq 40$ mm. The calculated values of induction component at $K0 = 0M = 40$ mm and current $I = 200$ A along axis 0_y at distance $z = (-10 - -40)$ mm are reduced with the increase of the distance to the elements with current (Figure 3, *a*), i.e. there is a gradient of the magnetic field inductance in these directions. If a ferromagnetic plate (item) is placed at distance $h = 20$ mm from the axis of the lower conductor $K0$ (see Figure 2), the tangential component of induction measured along axis 0_y located on the level $z = -10$ mm from the axis of conductor $K0$, is reduced 2 times, and that on level $z = -15$ mm (at 5 mm

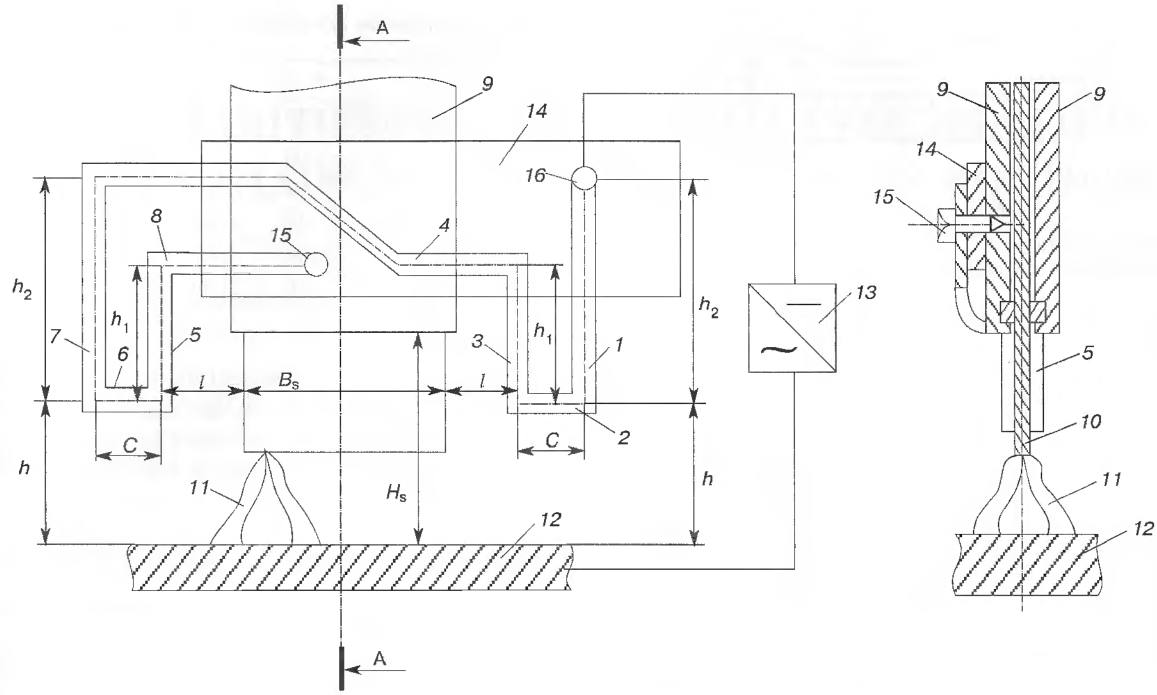

Figure 4. Device for current supply to the electrode for surfacing by magnetically-impelled arc (for symbols see the text).

distance from the item) is reduced 3 to 4 times (Figure 3, *b*). However, $|\Delta B_x|$ practically does not change in the presence of a ferromagnetic item. The induction component B_x at the surface of the ferromagnetic item can be increased by placing magnetic reflectors (from ferromagnetic sheet steel more than 0.5 mm thick and more than 30 mm wide) along the surface of element $0K$, the value increasing 2 to 3 times in this case. It is rational to use such shields in the devices also in the absence of the ferromagnetic item, i.e. in surfacing (welding) of items of non-magnetic materials.

In view of the above, a design of the device for current supply to the strip electrode has been proposed (Figure 4), consisting of the elements through which surfacing current I_s is flowing [5]. The axes of all the elements of the current conduit are located in the plane of the strip electrode (strip stick-out). Such distances l and h from axes of elements *5* and *6* of the device are optimal, at which not only the required induction gradient depending on the arc position at the strip tip (ΔB_x is maximal when the arc is at the strip edge) is provided, but also a certain level of additional induction for compensation of $|\Delta B_x|$ when the arc is at the strip edge (in $y = \pm 0.45\ B_s$ position). The upper edges of the sections of current conduits *1, 3, 5, 7* are bent out-of-plane to such a distance as to provide good contact between elements *4* and *8* and insulating gasket *14* which is attached to current-conducting tab *9*. Element *8* is connected to tab *9* by bolt *15*. The pole of the welding rectifier *13* is connected to the vertical section of the current conduit in point *16*. The electric circuit is closed to the other pole of rectifier *13* through item *12* and arc *11* during its arcing at the tip of strip *10*. The optimal dimensions of the device are: $h_1 = 50 - 80$ mm; $h_2 = h_1 + 30$ mm; $C = (0.6 - 0.8)\ h_1$ mm. The optimal values of distances l and h are selected from the condition of achievement of the required values of B_x and $|\Delta B_x|$ with the arc positioned at the strip edges. If B_x and $|\Delta B_x|$ are insufficient, they can be increased 2 times, applying two frames (two turns) instead of one shown in Figure 4, or magnetic shields mounted on elements *2, 3* and *5, 6* from the inner side of the frames. The above dimensions of the current conduit elements and distances $l = 5 - 10$ mm, $h = 20 - 25$ mm completely compensate $|\Delta B_x|$ in the arc zone at $H_s = 40$ mm and $B_s = 40 - 120$ mm (Table 1).

The effectiveness of the proposed device was checked by submerged-arc surfacing with strip electrode of 08kp steel 0.2 mm thick and 40 – 80 mm wide a plate of VMSt.3sp steel under AN-348A flux at reverse polarity direct current. The parameters of the surfacing modes were as follows: $U_a = 31 - 33$ V; $v_s = 20$ m/h (0.556 cm/s). Dimensions of the device were: $l = 10$ mm; $h = 25$ mm;

Table 1. Data on magnetic field simulation in the arc zone in surfacing with strip electrode ($I = 200$ A)

B_s, *mm*	$|\Delta B_x|$ *in the arc current pick-off zones (Figure 1, a), mT*		
	I	*II*	*III*
40	0	0	0
60	0	0.1	0.1
80	0	0.2	0.1
100	0	0.2	0.1
120	0	0.2	0.1

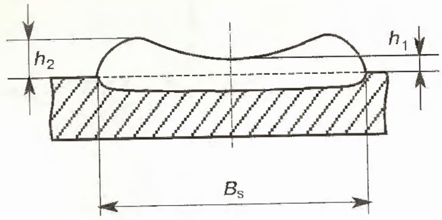

Figure 5. Schematic for determination of the criterion of the deposited bead formation quality.

h_1 = = 50 mm; C = 40 mm; h_2 = 70 mm. The criterion of the quality of bead formation is $\Delta h = h_1 - h_2$ parameter (Figure 5). The data (Table 2) confirm that the proposed device allows improvement of bead formation. Increase of surfacing current (required for wider strip) leads to greater values of $|\Delta B_x|$ formed by surfacing current flowing in the strip stick-put, this being completely compensated by the adequately increased but having an opposite sign values of $|\Delta B_x|$ formed by surfacing current flowing in the device elements.

Table 2. Data on the criterion of the deposited bead formation quality

Surfacing	B_s, *mm*	I_s, *A*	Δh, *mm*
Without the device	40	360 – 380	–2.20
	60	420 – 440	–2.00
	80	500 – 520	–2.10
With the device	40	360 – 380	–0.21
	60	420 – 440	0.00
	80	500 – 520	+0.20

CONCLUSIONS

1. The defect forming as a saddle in the central part of the bead in submerged-arc surfacing with the strip electrode, is of an electromagnetic nature and is connected with accelerated displacement of the arc from the center to the edges of the strip and displacement of liquid metal volumes to the side edges of the weld pool.

2. Application of controlling magnetic fields eliminating the gradient of the magnetic field induction in the arc zone, allows prevention of the saddle-type formation defect in the center of the bead deposited with the strip electrode.

REFERENCES

1. Kravtsov, T.G. (1978) *Electric arc surfacing with electrode strip*. Moscow: Mashinostroyeniye.
2. Razmyshlyaev, A.D. (1985) Study of liquid metal flows in arc welding. *Svarochnoye Proizvodstvo*, **10**, 31 – 32.
3. Razmyshlyaev, A.D., Maevskii, V.R. (1995) Pattern of the magnetic field in the interelectrode gap in arc surfacing with strip electrode. *Ibid.*, **2**, 15 – 18.
4. Razmyshlyaev, A.D. (1983) Arc displacement in submerged-arc strip surfacing. *Avtomaticheskaya Svarka*, **6**, 70 – 71.
5. Razmyshlyaev, A.D., Maevskii, V.R. *A device for current supply to the electrode for magnetically-impelled arc welding and surfacing*. USSR author's certificate **1704973**. Publ. 1992.

PECULIARITIES OF HEATING PARTS OF LIMITED SIZES IN GLOW-DISCHARGE DIFFUSION BONDING

G.P. BOLOTOV
Chernigiv Technological Institute, Chernigiv, Ukraine

ABSTRACT

Character of distribution of heat flows in parts of limited sizes in glow-discharge heating under conditions of diffusion bonding is analysed. The expediency of using heat-insulating spacers between a part and a clamp is shown. The precise and approximate solutions of the problem of temperature distribution in parts, depending upon thermal-physical and geometrical characteristics of base materials and spacers, are given.

Key words: diffusion bonding, glow discharge, finite bodies, heat-insulating spacers, heating, modelling.

The glow discharge characterized by technological flexibility is used to advantage for diffusion bonding of dissimilar materials in mass, small-scale or customized production of instrument units, machine parts, cutting and forming tools [1–3]. Frequent change of sizes and types of parts hampers control of one of the basic parameters of diffusion bonding, i.e. heating temperature, which has a dominant effect on the quality of the bonds.

Temperature measurement in the diffusion bonding zone involves certain difficulties. Errors in the measurement can amount to 100 K and more even in the case where thermocouples are used as the sensors [4]. It is suggested in [5] that the errors could be reduced by controlling the heating temperature of parts on the basis of the degree of their plastic deformation under compression loading. However, because diffusion bonding induces very insignificant deformations in the parts, this method, in addition to the fact that it requires more sophisticated equipment, fails to ensure the desirable accuracy of the measurements.

In the case of using the glow discharge, this problem is aggravated by a very high temperature amounting to 1500 – 3000 K, which prevents the use of the thermocouple sensors within the discharge-affected zone, and by optical interferences caused by emission of the plasma and contamination of the observation holes due to cathode sputtering of the materials of the parts, which limits application of the optical control methods (optical and photoelectric pyrometers).

Therefore, instead of direct measurement of the temperature within the bonding zone, its thermal state in a number of cases is controlled using mathematical models, which relate controlled and adjusted parameters of the heat source to the heating temperature of the parts joined. However, the available models [6, 7] were developed on the basis of a diagram of heating semi-infinite bodies, which limits their application field to items of certain sizes and shapes. At the same time, there are many items which cannot be regarded as unlimited bodies because of their geometrical parameters and character of distribution of heat flows in them. In particular, such items include bonded bimetal hard-alloy dies, glass-metal connections in RF waveguides [8], etc. These items are characterized by a large difference in sizes of the parts in a longitudinal (along the axis of application of the compressive load) direction. Thus, the size ratio of parts of the bimetal dies is 1/3 – 1/4, and while the steel holder can be assumed to be a semi-infinite body, the cutting hard-alloy part is extended only to 0.015 – 0.030 m (Figure 1). In this case the bonding zone *0–0* (the zone affected by the heat source) is located in an immediate vicinity to interface *I–I* between a part and a massive punch of the clamping device in contact with a water-cooled chamber casing. In the presence of a tight contact between them (interface *I–I* has no thermal resistance) an increased heat flow from part *2* to the clamping device makes it necessary to put an excessive energy into the bonding zone, which leads to substantial temperature gradients in this part. This situation can be tolerated neither by hard alloys nor by non-metallic materials.

To prevent energy losses at the clamping device and equalize temperatures along the length of part *2*, heat-insulating spacers of a low thermal conductivity material are placed between them. In the first approximation such a spacer can be considered to be an adiabatic (conducting no heat) boundary. In this case the heat flow, propagating from zone *0–0* of a maximum temperature and reaching interface *I–I*, will be reflected from it to cause an increase in temperature within the bonding zone *0–0*. According to recommendations given in [9], this reflection can be modelled by adding a heat source simulator (of the same power as the basic source)

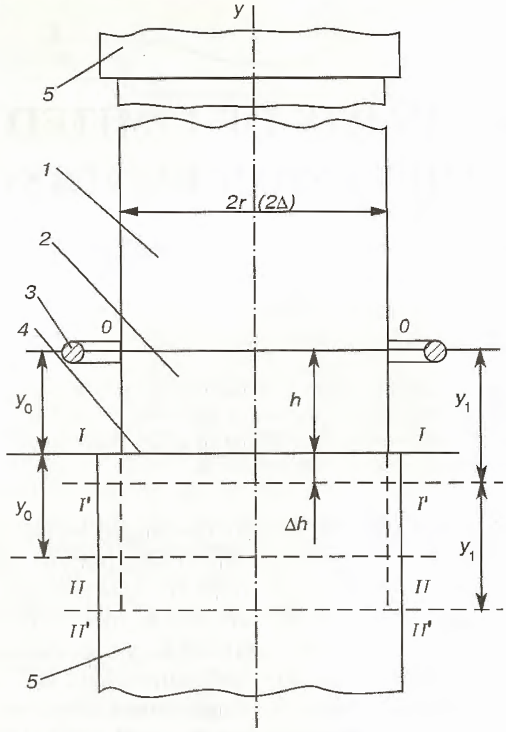

Figure 1. Diagram of glow-discharge heating of parts of different sizes: *1, 2* — parts joined; *3* — anode; *4* — heat-insulating spacer; *5* — clamping device punches.

to affect the other side of interface *I–I* at a distance of Δh from it (interface *II–II* in Figure 1). The distance between the bonding zone and the heat source simulator is $2y_0 = 2h$. Thickness of the heat-insulating spacer, being insignificant, is ignored.

By reducing, according to [7], the glow-discharge heating to a diagram of heating with a flat source acting within the bonding zone *0–0*, the temperature in this zone can be determined as follows:

$$T(t) = \frac{q}{2F\sqrt{\pi\lambda c\rho}} \times \left[\int_0^t \frac{dt}{\sqrt{t}} \exp(-bt) + \int_0^t \frac{dt}{\sqrt{t}} \exp(-(2y_0)^2/4at - bt)\right], \quad (1)$$

where q is the heat source power; F is the cross section area of the parts joined; λ is the thermal conductivity of the material of the parts; $c\rho$ is the material heat capacity by unit volume; b is the convective heat transfer; a is the thermal diffusivity and t is the heating time.

The augend in square brackets is an increase in temperature in the bonding zone caused by effect of the heat source, and the addend is the same caused by the heat source simulator.

Expression (1) corresponds to an ideal case, where interface *I–I* arrests the heat flow from the bonding zone. Under actual conditions, dehydrated mica or ceramics, having a comparatively low thermal conductivity λ_1 (0.40 – 0.58 for mica and 3.00 – 5.00 W/(m·K) for ceramics) at 1273 K are used as the heat-insulating spacers [10]. However, such spacers are of a small thickness (δ = 0.0003 – 0.0010 and 0.003 – 0.005 m for mica and ceramics, respectively), their thermal resistance $R_1 = \delta/\lambda_1$ has a finite value. Therefore, part of the heat flow coming to interface *I–I* will tend to penetrate through it and will be lost at elements of the clamping device. Under these conditions the heat flow reflected from interface *I–I* will be smaller than in the previous case; hence, the temperature within the bonding zone *0–0* will be lower than that calculated from expression (1). A decrease in the reflected heat flow is caused by the fact that the adiabatic interface shifts from the bonding zone to some distance of Δh to reach the position of *I′–I′*. Conventional shift of the interface is determined by capability of the heat-insulating spacer of arresting the heat flow that reaches interface *I–I* (and that preliminarily has passed through material of the part h long) and has a certain thermal resistance $R_2 = h/\lambda$, i.e.

$$\Delta h = \frac{R_2}{R_1} h. \quad (2)$$

The conventional adiabatic interface *I′–I′* is at the following distance from the bonding zone

$$y_1 = h + \Delta h.$$

In this case the heat source simulator is in position *II′–II′* at a distance of

$$2y_1 = 2(h + \Delta h) \quad (3)$$

from the bonding zone *0–0*, i.e. expression (1) describing temperature variations in this zone (at y = = 0) and along the part length will have the following form:

$$T(t) = \frac{q}{2F\sqrt{\pi\lambda c\rho}} \times \left[\int_0^t \frac{dt}{\sqrt{t}} \exp\left(-\frac{y^2}{4at} - bt\right) + \int_0^t \frac{dt}{\sqrt{t}} \exp\left(-\frac{(2y_1)^2}{4at} - bt\right)\right]. \quad (4)$$

The above form of expression (4), allowing for thermal-physical properties of the spacer, characterized by relationship (2), can be used to describe temperature variations in the bonding zone in the following cases:

1. $R_1 = 0$ (no spacer), $\Delta h \to \infty$, the integrand function in the addend tends to zero, which corresponds to bonding of two semi-infinite bodies. An increased heat removal to punches of the clamping device leads to a decrease in temperature within the bonding zone.

2. $0 < R_1 < \infty$, heat removal to the clamping device decreases, Δh has a finite value. Temperature

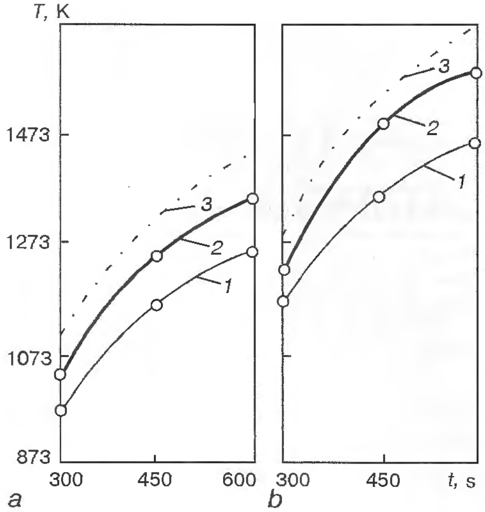

Figure 2. Values of current temperature of the bonding zone in parts of different sizes made from St.3 (*a*) and 12Kh18N10T (*b*) during glow-discharge heating: *1* — without spacer; *2* — experiment; *3* — numerical integration of expression (4).

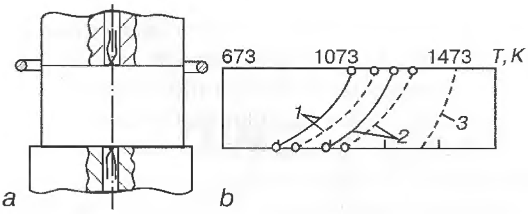

Figure 3. Schematic of the bonding zone (*a*) and dependence of temperature along the length of the part (12Kh18N10T) upon the heat-insulating spacer (*b*): *1* — without spacer; *2* — with spacer; *3* — ideal heat-insulating spacer; —— — experiment; - - - - — calculation.

in the bonding zone depends upon thermal-physical properties of the spacer.

3. $R_1 \to \infty$, $\Delta h = 0$, it is the case of the adiabatic interface *I–I*, which can hardly be achieved under actual conditions. The calculated values of the temperature are substantially higher than the actual ones.

The upper limit of integration, corresponding to the duration of heating the parts to a preset temperature, is assumed to be equal to $t_h = t - t_1$, where t_1 is the time of heating through the cross sections of the parts in their contact zone (after which we can assume the flat heat source to be formed in this zone). Time t_1 is determined on the basis of thickness of the thermal layer (radius of the parts r or their half-length Δ): $r = \sqrt{6at_1}$ [11].

Adequacy of the calculation model represented by expressions (2) to (4) was estimated by comparing it with results of heating the composite cylindrical samples, 0.028 m in diameter, of steels — St.3 and 12Kh18N10T – 12Kh18N10T. The components of the samples related to each other as 1 to 4 and the smaller component was 0.02 m long. Quartz glass 0.003 m thick was used as the heat-insulating spacer. Thermal conductivity of the quartz glass slightly depends upon the temperature and is 2.0 – 2.5 W/(m·K) for a temperature range of 373 – 1273 K [10]. The parts heated served as the cathode and the circular wire anode was located equidistant to the perimeter of their contact zone at a distance of 0.006 m from the surface of the parts. The temperature was controlled with the chromel-alumel thermocouple placed at two points at the opposite ends of the smaller part. Heating was done in nitrogen at a discharge current of 4 A, gas pressure of 5.32 kPa and load acting on the parts equal to 2 MPa.

The measurements were made with and without the heat-insulating spacer. Experimental values of the current temperature of the bonding zone of the parts (at $y = 0$) are given in Figure 2. The Figure also shows values of the temperature obtained by numerical integration of expression (4) by the Simpson method for time intervals of 300, 450 and 600 s. Conditional shift of the adiabatic interface for the St.3 and 12Kh18N10T samples is 0.0087 and 0.0130 m, respectively.

Figure 3 shows results of measurements of the temperature at the opposite ends of part *2*, corresponding to the time interval of $t = 300$ s. The measurements were made with and without the spacer. The results indicate that under the given conditions, i.e. in heating the parts of steel 12Kh18N10T, the temperature gradient varies along the length of the part *2* from 1.26 – 1.29 (at its direct contact with the punch of the clamping device) to 1.16 – 1.18 (at the presence of the spacer located between them and having the above thermal-physical and geometrical characteristics). An increase in thermal resistance of the spacer leads to further equalization of temperatures in the parts, which is proved by results of numerical integration of expression (4) for $R_1 \to \infty$ (Figure 3, curve *3*). Somewhat higher temperature gradients obtained by calculation methods (Figure 3, curves *1* and *2*), as compared with the actual values, are attributable to modelling the glow discharge as surface distributed heat source (flat) concentrated in the contact zone of the parts.

CONCLUSIONS

1. In glow-discharge bonding of parts of limited sizes, sensitive to non-uniform distribution of temperature in the bulk of them, the required temperature gradients can be achieved by using an appropriate heat insulation of the parts from elements of clamping devices. For this, it is necessary to make allowance for thermal-physical and geometrical characteristics of the spacers, which determine their thermal resistance.

2. Calculations from expression (4) show that in joining steel parts, for which distribution of heat can be assumed to be unidimensional, i.e. along the longitudinal axis (cylinder, parallelepiped and other bodies which can be reduced to them), and

for their extension in this direction equal to $h \geq \geq 0.04 - 0.05$ m, the heat flow reflected from the boundary opposite to their contact zone has an insignificant effect on the temperature of the bonding zone. Therefore, these parts can be assumed to be semi-infinite bodies, and the appropriate simplified calculation dependencies can be used to evaluate the temperature field in them.

3. The method suggested for determination of temperature fields in parts of limited sizes can find application also for other heat sources, heating with which can be reduced to the diagram of heating with a flat heat source, in particular, for induction heating with a single-turn induction coil.

REFERENCES

1. Kotelnikov, D.I., Bolotov, G.P., Sivakov, A.L. *et al.* (1985) Device for glow-discharge diffusion bonding of hard alloys to steels. *Avtomaticheskaya Svarka*, **7**, 71 – 72.
2. Mukha, I.M., Dovbishchuk, M.N. (1973) Restoration of hard-alloy fixture and tools by glow-discharge diffusion bonding. *Diffuzionnoye Soyedineniye v Vakuume*, **6**, 166 – 172.
3. Sadovnikov, B.V., Stepanov, G.N., Romanenkov, A.P. (1982) Glow-discharge diffusion bonding of hard alloy to steel using a prototype of the commercial diffusion bonding machine. *Elektrotekhnicheskaya Promyshlennost. Electrosvarka*, **4**, 21 – 22.
4. Chistyakov, Yu.A., Gorysheva, E.V. (1982) Errors in measuring the diffusion bonding temperature. *Svarochnoye Proizvodstvo*, **7**, 11 – 12.
5. Sivakov, A.L. (1989) *Device for controlling parameters of diffusion bonding in glow-discharge plasma*. Synopsis of Thesis of Cand. Sci. (Eng.). Leningrad: SZPI.
6. Frolov, A.P., Mashkova, N.A., Shishkova, A.P. *et al.* (1973) Some peculiarities of distribution of temperature in a cylindrical sample during induction heating under diffusion bonding conditions. *Diffuzionnoye Soyedineniye v Vakuume*, **5**, 72 – 81.
7. Chernysh, V.P., Bolotov, G.P., Kutepov, Yu.N. *et al.* (1984) Estimation of heating temperature in glow-discharge diffusion bonding. *Avtomaticheskaya Svarka*, **9**, 54 – 56.
8. Kotelnikov, D.I. (1972) Calculation of optimal conditions of solid-state bonding of glass to metal. *Ibid.*, **9**, 27.
9. Rykalin, N.N. (1951) *Calculation of heat flows in bonding*. Moscow: Mashgiz.
10. Musin, R.A., Konyushkov, G.V. (1991) *Joining metals to ceramic materials*. Moscow: Mashinostroyeniye.
11. Belyaev, N.M., Ryadno, A.A. (1978) *Non-stationary thermal conductivity methods*. Moscow: Vysshaya Shkola.

PILOT PLANT FOR WELDING CONSUMABLES TODAY

Pilot Plant for Welding Consumables (PPWC), which is a division of the E.O. Paton Electric Welding Institute of the National Academy of Sciences of Ukraine, is one of the largest manufacturers of welding consumables in Ukraine, both in volumes of production and in ranges of products. The Plant was founded in 1977 on the base of electrode production of the Pismennyj Metalware Association. That facility had been producing electrodes for manual arc welding since 1947. The team formed at the Plant had large experience in manufacturing the most common types of welding consumables. There has been a many-year fruitful cooperation between specialists of the Plant and a number of leading departments of the PWI, aimed at the manufacture of new types and grades of electrodes developed at PWI and intended for commercial application in different industries.

Reconstruction of the Plant in 1959 – 1964 resulted in building of basic facilities for the manufacture of electrodes. The workshops were fitted with domestic equipment, which was most advanced to date: chipping machine tools PRA-4 and IAO-32, electrode covering presses OSZ-3 and AOE-3, conveyer-type drying-baking furnaces OKB-463, etc. The Plant produced 28 grades of general- and special-application electrodes. The annual output of electrodes amounted to 20,000 t.

During the first years since the foundation of PPWC the challenge was to arrange in the vacated and newly built premises the workshops for the manufacture of experimental and commercial batches of consumables for mechanized arc welding and hardfacing, such as flux-cored wires, fused and ceramic fluxes, solders, etc. This challenge was handled to advantage by the staff of the Plant. The workshops were started up with an active technical assistance and direct participation by the leading specialists of the PWI, and fitted with the domestic mass-production and customized equipment. In parallel with building the new workshops, upgrading was done to the existing electrode production. Indoor storehouses were constructed for raw materials and finished products, a section for preparation of liquid glass and covering materials for the manufacture of special electrodes was reconstructed, the conveyer furnace OKB-463 for the manufacture of the 3.0 mm diameter electrodes was re-equipped and the new chamber furnaces designed and fabricated at the Plant for baking special electrodes were put into operation.

Today the Plant has capacities for producing annually 12,000 t of general- and special-application electrodes, 500 t of flux-cored wire and 150 t of each of fused and ceramic fluxes. It should be noted that by the end of 1990 the Plant produced 32 grades of electrodes, 40 grades of flux-cored wires for welding and hardfacing and 25 grades of fused and ceramic fluxes.

Unfortunately, as a result of a general economy decline caused by disintegration of the USSR in the 1990s, the demand in Ukraine for mechanized welding consumables drastically decreased, which eventually led to a substantial reduction in volumes of their production by the Plant. In connection with the expected recovery of the economy in Ukraine, there is good reason to hope that the situation will gradually improve, the demand for consumables will grow and their output will increase. Pending these improvements, the equipment for production of flux-cored wires and fluxes is maintained in good

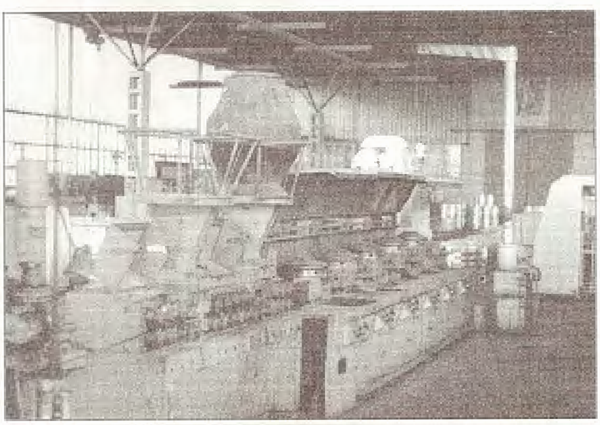

Section for production of flux-cored wire

Section of the workshop for processing of raw materials

working condition. Therefore, the Plant is prepared to resume production of any grades of these consumables as soon as it receives orders.

Despite the current unfavourable economical conditions the manual arc welding electrodes have remained in demand in the market of Ukraine and other CIS countries. Their production volumes have also been negatively affected by the decline, although the extent of this effect turned out to be smaller. Thus, in 1998 the Plant produced 10,000 t of electrodes and in 1999 their output was a bit over 8,000 t.

To preserve and strengthen its position in the market of electrodes and to increase competitiveness of the products, managers and engineering staff of the Plant pay a continual attention to measures aimed at raising the technical level of the electrode production, improvement of vendibility and performance of the electrodes on condition of keeping the prices at an affordable level. Despite the financial difficulties, the Plant managed to retool the electrode production facilities by installing new equipment.

One of the achievements of the Plant was building of a new workshop for processing raw materials. Two new electric drum-type and chamber furnaces for drying components delivered for preparation, jaw crushers SMD-08, ten reversing mills of the in-house design and manufacture and mills with continuous screening were installed in the workshop. Each mill is equipped with vibrosieve SV-2-06. Owing to the use of the new ball mills, the components have a consistent desirable mesh size. Two vibrosieves SV-2-09 are utilized to control classification of materials delivered to the Plant in the milled form. One of them is equipped with a device for unpacking large bags. Comprehensive measures were taken to prevent ingress to the workshop of harmful dust formed during technological operations. Available is a large number of special hermetically sealed containers for storage and transportation of crushed materials and finished powders. The prepared components are loaded into the special containers for milled materials. Each container is inspected at the Quality Control Department, sealed and transferred to the central storehouse. When necessary, the materials are delivered to the weighing lines of the electrode production workshops.

Because of the absence in the market of reliable inexpensive straightening-chipping machine tools, the Plant periodically upgrades the available straightening-cutting machine tools PRA-4 and I6220. This allows an improvement in accuracy and quality of chipping of welding wire. The mechanized line for weighing the charge components has been put into operation at the special electrode production workshop to replace manual weighing.

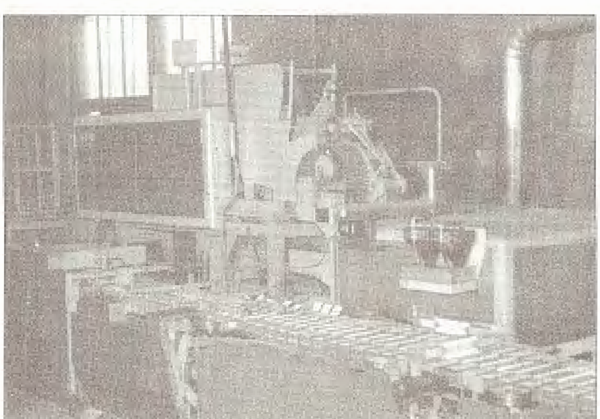

Machine for mechanized weighing and packing of electrodes

In the last years a great consideration has been given to improvement of quality of manual packing of the electrodes. The Plant is one of the first among domestic manufacturers to pack stick electrodes into cardboard boxes with the Plant trade mark. Special machines designed and manufactured at the Plant for the purpose are used for gluing the boxes. At the same time, the Plant successfully uses the Czech machines for mechanized weighing and packing the electrodes 3 and 4 mm in diameter. It is planned that by the end of this year all boxes used to pack electrodes will be hermetically sealed using a thermosetting film.

The great consideration at the Plant is given to improvement of methods and means for quality control of the consumables. The multi-channel quantometer SPM-25 is used to advantage to control composition of the deposited metal, raw materials delivered to the Plant and electrode charge.

The Plant has recently expanded the range of new grades of the electrodes developed by specialists of the PWI. These electrodes are characterized by high welding-technological properties, provide the sound weld metal and feature high adaptability for commercial manufacture. These are the electrodes of the ANO-27, ANO-TM, ANO-TM60 and ANO-TM/SKh grades. Worthy of notice is a joint development of the Plant and the Institute — the ANO-6U grade electrodes with an ilmenite covering of the E46 type, which are very popular among customers.

One of the key factors in improvement of the quality is certification of the Plant products in compliance with the UkrSEPRO system.

The UONI 13/45, UONI 13/55 and ANO-6 grade electrodes have received approval by the Sea Register.

During this year the Plant will focus on completion of development and introduction of the electrode manufacture system based on ISO standards, series 9000, which will allow our products to be brought to a new quality level. To realize these plans, the Plant pays much attention to training its engineering and technical staff in the field of quality assurance.

We hope that the efforts made by the Plant will allow us to preserve and strengthen our position in the market of welding consumables.

P.A. KOSENKO
Director
PPWC of E.O. Paton Electric Welding Institute

For more information, please contact:

2, E.Teligi,
Kyiv, 04112, Ukraine
Tel.: (38044) 456 63 69
Fax: (38044) 456 50 01

FORMATION OF DEPOSITED METAL ON INCLINED AND VERTICAL SURFACES

I.A. RYABTSEV, Yu.M. KUSKOV and **Ya.P. CHERNYAK**
The E.O. Paton Electric Welding Institute, NASU, Kyiv, Ukraine

ABSTRACT

The effect of surfacing conditions, compositions of charges of flux-cored wires and fluxes on the formation of a horizontal bead on inclined and vertical surfaces is experimentally investigated. It is shown that deposition on such surfaces should be done at a minimum possible amperage and maximum speed. The best choice for surfacing is the short flux of the AN-15M grade. The $CaCO_3$–CaF_2–TiO_2 gas-slag forming system with a component ratio of 3:1:1 provides the best results in the manufacture of self-shielded flux-cored wire.

Key words: *surfacing, inclined surface, bead, molten pool fluidity, surface tension, bead cross section asymmetry.*

Surfacing of some large-sized parts of complex configurations (casing parts of mining machines, large-module helical gears, U-shaped tram rails, etc.) involves difficulties associated with positioning of the surface to be treated to make it convenient for treatment. In these cases surfacing has to be done on inclined or vertical surfaces. However, this hampers good bead formation, because the deposited metal flows down and thus decreases the quality of treatment and increases costs of the surfacing operations, associated with the necessity of removing and chipping out large amounts of metal during machining.

In a general case, position of the surface of the molten metal pool and, thus, character of the deposited bead formation depend upon the following forces and the following directions of their action: gravity, pressure of the arc column, surface tension, electromagnetic force and reaction of the solid walls of the molten pool. Under the effect of these forces the pool metal flows, tending to take a position that would meet the condition of dynamic equilibrium.

This article considers the effect of some surfacing parameters and compositions of charges of flux-cored wires and fluxes on fluidity of the molten metal pool and, therefore, on character of formation of the horizontal beads deposited on inclined and vertical surfaces.

It is practically impossible to evaluate the individual effect of each of these factors on fluidity of the molten metal pool, especially so that this fluidity is restricted not only by these factors, but also by a rapid loss of mobility of molten metal caused by a high solidification rate. Therefore, the majority of the available experimental procedures allow evaluation of fluidity of the molten metal pool as a rule in complex. For the investigations we chose a procedure suggested in [1]. Its main point is that a horizontal bead is deposited on the inclined surface (inclination angle 35 – 40°) of a sample. Cross section of the bead is asymmetrical, which is caused by fluidity of the pool (Figure 1). The ratio of surface areas of the lower and upper parts of the bead is $\gamma = F_1/F_2$ (with respect to the asymmetry axis) and can serve as the characteristic of fluidity of the molten pool.

Analysis shows that, other conditions being equal, in deposition of horizontal beads on inclined or vertical surfaces the probability of flow down of the pool metal is determined by the relationship between the gravity and surface tension forces. Besides, as the molten metal pool increases in size, its volume and, accordingly, mass increase much

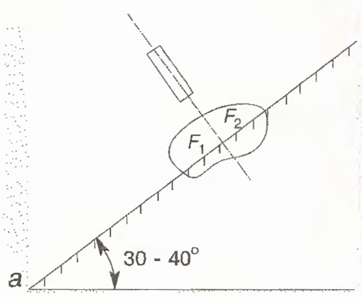

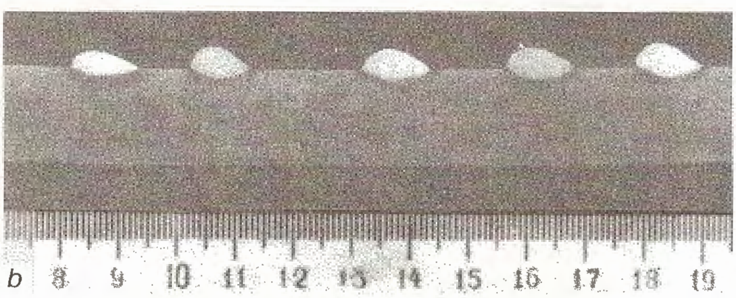

Figure 1. Schematic of measuring fluidity of the molten metal pool (*a*) and macrosection of the beads (turned) deposited on the inclined surface using different wires (*b*).

faster than its surface. As a result, there comes the moment when the surface tension force can no longer keep the pool and its metal starts flowing under gravity.

Volume of the molten metal pool depends firstly upon welding (surfacing) conditions. Therefore, from the beginning it was the effect of the amperage and surfacing speed on fluidity of the pool that was evaluated to select optimal surfacing parameters for conducting the designed experiments. The experimental model flux-cored wire of the PP-Np-20KhG grade with a diameter of 2.6 mm was used for the experiments. The wire was made in two versions: for submerged-arc surfacing using the AN-348A flux and for open-arc surfacing. The surfacing speed was varied from 10 to 35 m/h at a current of 350 A, while the current was varied from 250 to 450 A at a surfacing speed of 20 m/h. Results of measurements of fluidity of the pool, γ, calculated as a mean value over not less than five cross sections of the deposited beads are shown in Figure 2. Lower surfacing speed corresponded to a higher pool fluidity. In self-shielded wire surfacing the pool fluidity was the highest for the entire range of the speed values (Figure 2, *a*). At a speed of 10 m/h the pool could not be kept. The experiments for selection of the optimal value of the electric current were conducted at a surfacing speed of 20 m/h. Certain stabilization of the pool fluidity was observed at a higher speed value. As might be expected, an increase in the electric current was accompanied by an increase in the pool mass and fluidity (Figure 2, *b*). The satisfactory bead formation in surfacing using both types of wire (self-shielded and that used for submerged-arc surfacing) was produced at a current of 300 – 350 A, although the pool fluidity in self-shielded wire surfacing was higher.

Further experiments to investigate the effect of charges of flux-cored wires and fluxes on fluidity of the molten metal pool in deposition of horizontal beads on inclined and vertical surfaces were conducted under the following conditions: current 300 – 350 A, voltage 26 – 28 V and surfacing speed 20 m/h.

The investigations began with evaluation of the effect of composition of the gas-slag forming system of self-shielded flux-cored wires on fluidity of the molten metal pool. The system which is most widely used for the manufacture of surfacing self-shielded flux-cored wires is $CaCO_3$–CaF_2–TiO_2. The following ratios of components (minerals) are recommended: 1:2:3 (marble–fluorspar–rutile) [2, 3] or 2:5:3 (marble–fluorspar–perovskite) [4, 5].

It is a known fact [6] that an increase in the TiO_2 content causes a decrease in surface tension of slags due to the formation of complex anions TiO_3^{2-} with a large radius and a low electric charge, which slacken the bond between particles of the

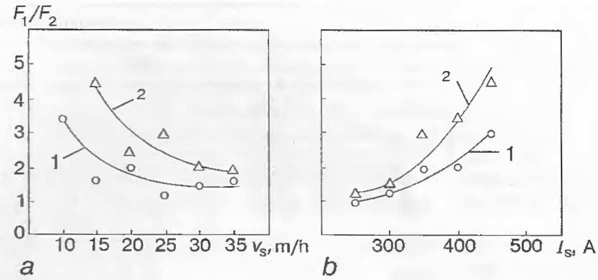

Figure 2. Dependence of fluidity of the molten metal pool on the surfacing speed (*a*) and amperage (*b*): *1* — submerged-arc surfacing using flux-cored wire; *2* — same using self-shielded wire.

melt. And vice versa, an increase in the content of strong oxides CaO and MgO causes an increase in surface tension of the slag melt due to an increase in the binding energy of ions as a result of an increase in the concentration in the melt of strong cations Ca^{2+} and Mg^{2+}, as well as oxygen anion O^{2-}. With an increase in the concentration of anions O^{2-}, due to a decrease in that of anions F^-, the binding energy of ions grows to cause an increase in the surface tension force.

Similarly, TiO_2, CaO and MgO affect tension between the phases at the metal–slag interface in the CaF_2 + TiO_2 and CaF_2 + CaO binary systems [7]. Therefore, to increase surface tension and tension between the phases at the metal–slag interface in the $CaCO_3$–CaF_2–TiO_2 system, it is necessary to increase the marble content and decrease the rutile content. However, as noted in [4], in surfacing using self-shielded flux-cored wire, an increase in the marble content of the charge causes losses of metal for spattering and deterioration of melting properties.

Also, it is necessary to take into account the two-sided effect of a third component of the gas-slag forming system, i.e. fluorides, on operational properties of self-shielded flux-cored wires. They are added to the wire charge to prevent hydrogen-induced porosity of the deposited metal. However, according to data given in [8], the fluoride content of more than 1 % results in degradation of quality of the deposited metal formation.

On this basis and proceeding from the experiments conducted, the ratio of components equal to 3:1:1 (at their total content of about 5 % in the flux-cored wire charge) was selected for the $CaCO_3$–CaF_2–TiO_2 system, which provided good performance of the self-shielded flux-cored wire.

Experimental verification of fluidity of the molten pool in surfacing using self-shielded flux-cored wire with a gas-slag forming system of the $CrCO_3$–CaF_2–TiO_2 type and a ratio of components equal to 1:2:2 and 3:1:1 showed that in the first case γ = = 1.86 and in the second — 1.67. On this basis, it can be concluded that for surfacing on inclined and vertical surfaces the better choice is to use self-shielded flux-cored wires with the $CaCO_3$–CaF_2–

Flux-cored wire No.	Content of elements, wt. %							Molten pool fluidity
	C	Si	Mn	Cr	Mo	P	Cu	
1	0.05	0.55	1.02	–	–	–	–	1.40
2	0.24	0.46	0.93	–	–	–	–	1.98
3	0.47	0.50	0.98	–	–	–	–	2.14
4	0.46	0.50	0.95	2.62	–	–	–	1.67
5	0.52	0.52	1.00	5.70	–	–	–	1.65
6	0.49	0.49	0.96	9.07	–	–	–	1.70
7	0.48	0.53	0.90	8.50	–	–	0.55	2.21
8	0.50	0.46	0.97	7.96	–	–	0.92	2.35
9	0.48	0.50	1.03	8.10	–	–	1.80	2.42
10	0.51	0.45	0.96	7.85	1.80	0.10	–	1.59
11	0.46	0.48	0.96	8.00	1.96	0.24	–	1.72
12	0.49	0.47	1.03	8.23	1.92	0.40	–	1.95

TiO_2 gas-slag forming system and a component ratio of 3:1:1.

It would be interesting to use this procedure to investigate the effect of fluxes, which are most commonly applied for surfacing operations, such as AN-348A, AN-15M, AN-20 and AN-26, on fluidity of the molten metal pool. The model flux-cored wire of the PP-Np-20KhG grade was utilized for the experiments. It was found that the AN-15M flux provided the lowest fluidity of the molten pool: $\gamma = 1.40$. The rest of the investigated fluxes had the following fluidity characteristics: AN-26 — 1.53, AN-20 — 1.74, AN-348A — 1.83.

As it is known from [9], the fluxes investigated have roughly the following melting point ranges, °C: AN-15M — 1300 – 1350, AN-26 — 1380 – 1430, AN-348A — 1320 – 1380, AN-20 — 1200 – 1250. Besides, the AN-15M and AN-20 fluxes are short and the AN-26 and AN-348A fluxes are long.

The lowest fluidity characteristics in submerged-arc surfacing using the AN-15M flux can partially be explained by the fact that it is short and has a sufficiently high solidification point. In addition, it contains a large amount of calcium oxide (29 – 33 %) which, as indicated above, causes an increase in surface tension of the slag melt and tension between the phases at the slag-metal interface. Although the AN-20 flux is also short, its fluidity characteristic is rather high. This could be explained by the fact that it has a relatively low solidification point. In addition, as compared with the AN-15M flux, in the AN-20 flux the content of CaO, which causes an increase in surface tension, is several times lower, and the content of silicon dioxide, which causes a decrease in surface tension, is almost twice as high [7].

The metal deposited using the AN-348A flux, which contains a large amount of silicon dioxide and manganese oxide, causing a decrease in surface tension of the slag melt and the metal–slag interface tension, exhibited the highest fluidity [7].

The middle place in characteristics of fluidity of the molten metal pool is taken by the AN-26 flux, which belongs to long fluxes but, as compared with AN-348A, contains a smaller amount of silicon dioxide, causing a decrease in surface tension, and a larger amount of magnesium oxide, causing an increase in surface tension.

The procedure accepted was used to investigate the effect of carbon, chromium, copper and phosphorus on fluidity of the molten metal pool. The choice of these elements was based on the following factors. Hardness and wear resistance of the deposited metal depend primarily upon carbon and chromium contents. Copper is a promising alloying element which provides an improvement in performance of the deposited metal. Its addition to precipitation-hardening steels causes an increase in hardness of HRC_e 10 – 15 [10]. Initial experiments showed that wear resistance of the deposited metal could be increased, avoiding a significant decrease in its crack resistance, by adding to it up to 0.5 % phosphorus. To eliminate precipitation of phosphides in the form of low-melting point eutectics along the grain boundaries, the deposited metal was alloyed with molybdenum, which promoted formation of the globular type of phosphides uniformly distributed in the steel structure [11].

The investigations were also conducted on surfacing using self-shielded flux-cored wires with different chemical compositions, but with the same $CaCO_3$–CaF_2–TiO_2 gas-slag forming system at a component ratio of 3:1:1, which ensured the lowest fluidity of the molten metal pool (Table).

Carbon (wires No. 1 – 3) causes an increase in fluidity of the molten metal pool, as it belongs to surface-active elements: an increase in its content is accompanied by a substantial decrease in surface tension [7]. Some effect on fluidity of the pool can be exerted by a decrease in the solidification temperature of steel with an increase in the carbon content. Over the ranges investigated, chromium (wires No. 4 – 6) has almost no effect on fluidity of the pool. This seems to be caused by the fact that it exerts a very insignificant effect on surface tension of steel [12 – 13]. The additions of copper increase fluidity of the pool, although further an increase in its content hardly causes an increase in fluidity (wires No. 7 – 9). Phosphorus is a surface-active element [7]. Thus, an increase in its content leads to a decrease in surface tension and increase in fluidity of the molten metal pool (wire No. 10 – 12).

Therefore, formation of the horizontal beads deposited on inclined and vertical surfaces can be controlled by varying surfacing parameters and compositions of charges of the flux-cored wires and fluxes. Deposition on such surfaces should be done at a minimum possible amperage and maximum speed. The best choice for surfacing is to use the short AN-15M flux. As to the self-shielded flux-cored wire, the best results were obtained with the $CaCO_3$–CaF_2–TiO_2 gas-slag forming system at a component ratio of 3:1:1.

REFERENCES

1. Erokhin, A.A. (1973) *Principles of fusion welding*. Moscow: Mashinostroyeniye.
2. Mikaelyan, G.S., Kasatkin, O.G. (1983) Selection of composition of the gas-slag forming system of flux-cored wire for surfacing on internal surfaces of parts. Surfacing of wear and heat-resistant steels and alloys. In: *Surfacing consumables*. Kyiv: PWI.
3. Zelenova, V.I., Ioffe, I.S., Erokhin, A.A. (1979) Effect of design of flux-cored wire on transfer of alloying elements from the wire charge at a stage of droplet. *Avtomaticheskaya Svarka*, **1**, 39 – 40.
4. Bilyk, G.B., Karpenko, V.M., Dorofeev, Yu.D. *et al.* (1979) Optimization of composition of gas-slag forming components of self-shielded wire. *Ibid.*, **2**, 48 – 50.
5. Bilyk, G.B., Karpenko, V.M. (1980) Indicators of melting in surfacing using self-shielded flux-cored wire. *Ibid.*, **1**, 57 – 58.
6. Shono, S.A., Kassov, D.S., Karpenko, V.M. (1977) Investigation of properties of slags for surfacing using self-shielded flux-cored wire. In: *Theoretical and technological aspects of surfacing*. Kyiv: PWI.
7. Yakobashvili, S.B. (1970) *Surface properties of welding fluxes and slags*. Kyiv: Tekhnika.
8. Krivchikov, S.Yu., Zhudra, A.P., Petrov, V.V. (1998) Effect of fluorides on welding-technological properties of self-shielded flux-cored wires. *Avtomaticheskaya Svarka*, **7**, 26 – 28.
9. Potapov, N.N. (1979) *Principles of selection of fluxes for welding of steels*. Moscow: Mashinostroyeniye.
10. Leshchinsky, L.K., Oldakovsky, A.I., Malinov, L.S. *et al.* (1981) Precipitation-hardening alloy of the 30Kh5G3D2MF type for wear-resistant surfacing. Theoretical and technological principles of surfacing. In: *Surfacing in machine-building and repair*. Kyiv: PWI.
11. Funahashi. Y. (1983) Conditions of precipitation and morphology of phosphides in three-component steels of the Fe–Me–P type. *J. Iron and Steel Inst. Jap.*, **12**, 1049.
12. Kolesnikov, T.P., Samarin, A.M. (1956) Effect of manganese, chromium and vanadium on surface tension of molten iron. *Izv. AN SSSR. Division of Engineering Sciences*, **5**, 66 – 67.
13. Tsarevsky, B.V., Popel, S.I. (1960) Effect of alloying elements on surface properties of iron. *Izv. Vuzov. Non-Ferrous Metallurgy*, **12**, 12 – 16.

STRUCTURE OF WELDED JOINTS FROM LOW-ALLOYED HEAT-RESISTANT Cr–Mo–V PEARLITIC STEELS

V.V. DMITRIK
Ukrainian Engineering and Pedagogical Academy, Kharkiv, Ukraine

ABSTRACT

Peculiarities of technology of CO_2 automatic welding of structures from heat-resistant Cr–Mo–V pearlitic steels are considered. Technology is based on the results of modelling of temperature conditions of the welding process and provides structure in welded joints which is close to optimum.

Key words: *arc welding, heat-resistant steels, optimum structure, modelling, temperature conditions.*

To increase the service life of welded structures of low-alloyed Cr–Mo–V heat-resistant pearlitic steels (including 15Kh1M1F and 12Kh1M1F grades) it is actual to provide the formation of their optimum initial structure, i.e. structure formed directly after welding and post heat-treatment , that is an aim of the present work.

It follows from [1, 2] that the optimum structure of the weld metal for the mentioned steels is ferritic-pearlitic or bainitic-ferritic with a fine ferritic fringing at the grain boundaries. In accordance with [3] the optimum (acceptable) structure of steels of 15Kh1M1F and 12Kh1M1F grades is a structure which contains 30 % of ferrite and the rest is bainite. In opinion of M.V. Pridantsev and K.A. Lanskaya [4], and also of the author of the present article, it is possible to obtain the increase in level of a creep resistance and ductility by providing the minimum sizes of a ferritic grain (≤ 15 μm) in bainite or by imparting the acicular form to it.

Analysis of fractures of welded joints from these steels showed that the initiation and beginning of crack propagation occur at those regions whose structure is differed from optimum (including those having a structural inhomogeneity).

It is known that in multipass welding of thick-walled structures at conventional conditions there appears a need in their additional preheating to the temperatures recommended by standard documents (SD) because of an intensive surface heat dissipation from the regions of edge preparation. Here, due to accumulation of heat in the deposited metal the overheating of separate regions of the weld metal and HAZ can be observed. During manufacture of welded structures, their temperature conditions are corrected by the thermocouple measurement data to correspond to the requirements of SD. However, to obtain the quantitative pattern of temperature conditions in welded joints to provide the necessary conditions for the formation of optimum initial structure of the metal of joints is possible only on the basis of modelling.

Optimum initial structure can be produced only if the SD are kept by welding at heat inputs which correspond to the data of modelling of the temperature conditions in the welded joints. Method, developed by us, for determination of the temperature conditions in the region of the pool melt (solidifying zone of weld metal and HAZ), including the solution of a mating heat problem [5 – 7], provided for the first time the sufficient accuracy in calculation data for prediction of the forming structure of the welded joint metal.

The mathematical model of the given problem included its numerical solution by using the method of iterations in the conditions of Navier–Stokes law (liquid phase) with a next solution of the Stefan problem in the conditions of Fourier law (solid phase). Using special basic functions (method of Galerkin) in the model structure allowed, by their decomposition in section of welded joints, the isotherms to be obtained which characterize the regions of liquid and solid phases during cooling and also the regions of HAZ in coordinates.

As a result of modelling the temperature conditions it was established that the metal regions with a structure, not meeting the requirements of SD [8–10], can be formed in welded joints made even without their violation. The regions of these structures are formed due to overheating of the deposited and parent metal, i.e. they are caused by its long duration within the region of temperatures of γ-phase, close to the melting temperature. The heating intensity and the appropriate duration of the metal in an austenitic state provide a certain inhomogeneity of the austenite.

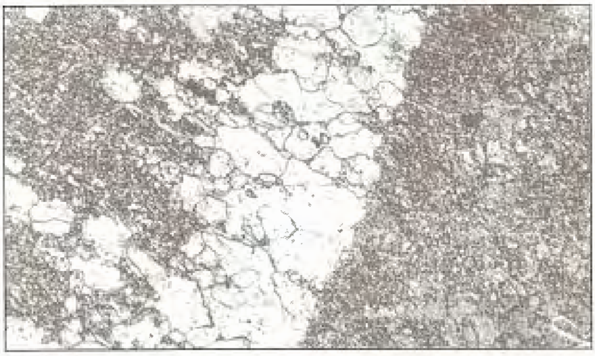

Figure 1. Microstructure of fusion region of HAZ. Mechanized welding in CO_2, steel 15Kh1M1F (×100) (reduced by 0.80).

It was established that due to overheating, for example, in the fusion region (mainly in thick-walled structures) the local ferritic interlayers may occur (Figure 1). Their revealing, including the use of non-destructive methods of control (ultrasonic testing), is not possible because of their small size and a local nature. Here, the structural inhomogeneity (presence of soft interlayers) promotes the reduction of characteristics of mechanical properties (Figure 2) [11]. Value of *KCU* with a notch in the fusion region is 9 – 11 J/cm^2, that is lower than the requirements of SD.

Let us consider another example. In mechanized and automatic welding in CO_2 using the conventional conditions the overheating of regions revealed by calculations in a multilayer weld metal and HAZ (chemical composition is given in Table) was approximated across their section (Figures 3 and 4).

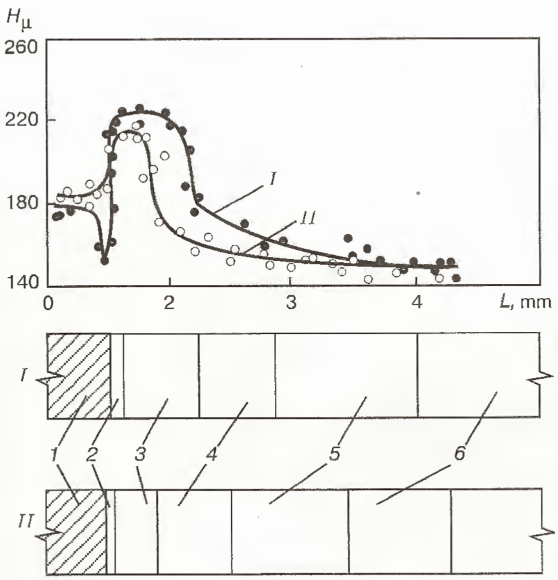

Figure 2. Microhardness of welded joints: *I* — mechanized welding in CO_2 at conventional conditions; *II* — automatic welding at recommended conditions; *1* — weld metal; *2* — fusion region; *3* — overheating region; *4* — region of normalizing; *5* — region of partial recrystallization; *6* — region of recrystallization; *L* — length of HAZ.

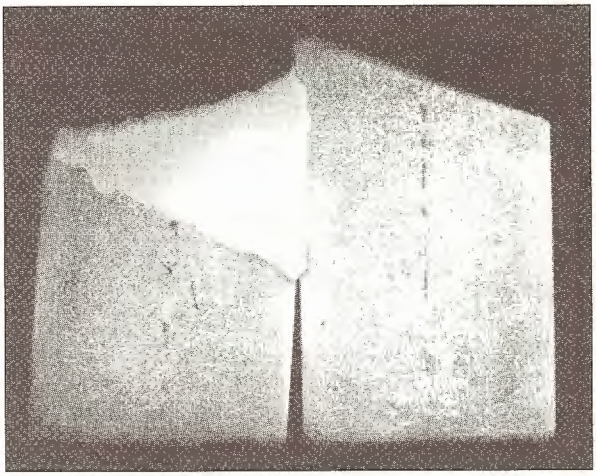

Figure 3. Macrostructure of transverse section of welded joint. Automatic welding in CO_2, steel 15Kh1M1F (×1.1) (reduced by 0.50).

It was determined that the overheating regions with ferritic interlayers in the fusion region of HAZ of the mentioned steels can have the length approximately from 30 μm to 0.5 mm and consist of separate local-grouped grains of the ferrite similar to those which are given in Figure 1, displaced from the fusion region towards the weld metal. Ferritic grains can be of different sizes (from 15 to 150 μm). The ferritic interlayers have a lower creep resistance as compared with that of the weld metal and parent metal including the HAZ metal (without taking into account the metal of the region of a partial recrystallization). Post heat treatment (for example, tempering at 730 °C, 3 h) does not essentially influence their structure and properties.

The processing of simulation data showed that the structure of the interlayers can change from ferrite to martensite depending on the physical nature of the temperature conditions and chemical composition of the deposited and parent metal. In

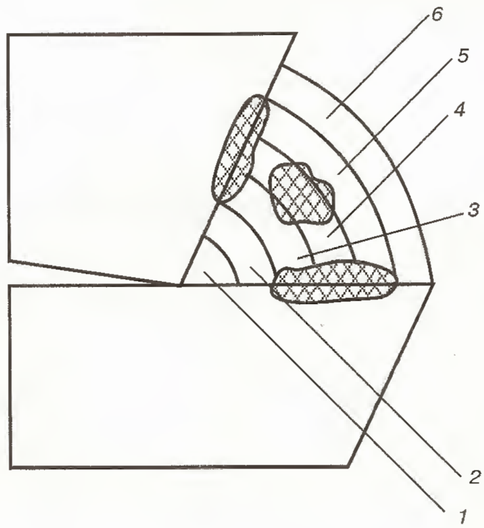

Figure 4. Scheme of transverse section of welded joint (corresponds to Figure 3): *1* – *6* — layers of a multilayer weld metal; regions of overheating are hatched.

Sampling	Elements, mass. %							
	C	Si	Mn	Cr	Mo	V	P	S
Parent metal (steel 15Kh1M1F)	0.14	0.15	0.62	1.25	1.0	0.25	0.012	0.019
Weld metal	0.10	0.35	1.22	0.90	0.5	–	[illegible]	0.020

[12, 13] the formation of martensitic interlayers relative to welding pearlitic steels with austenitic filler material is grounded. The estimated testing of these grounds taking into account the temperature conditions and gradients of chemical potentials of alloying elements [3, 13, 14] showed the feasibility of its application under the appropriate conditions and for the Cr–Mo–V steels used by us.

It was established that the formation of ferritic interlayers is promoted by silicon, which «repels» carbon, and, from our data, vanadium, which «attracts» carbon as a strong carbide former available in parent metal and absent in the deposited metal. The formation of strong VC carbides begins during cooling directly from the temperature of γ-phase, close to the primary crystallization. Similar interlayers can be formed also in manual arc welding under conventional conditions, including those when vanadium is present in weld metal (for example, at $V \leq 0.2$ %).

It is known [1, 12] that the formation of similar interlayers is controlled by two interrelated factors: chemical composition and temperature conditions of the deposited metal and parent metal (fusion region). In addition, in our opinion, the temperature conditions, i.e. relative share of interlayers depends on the degree of heat input into the parent metal, is a prevailing parameter in welded joints having parent and weld metal which is similar in composition.

Revealing of similar interlayers in the whole geometry of the fusion region, and also their prevention is effective only due to the modelling of temperature conditions in the welded joint. We should also note that application of numerical methods of finite differences and finite elements did not allow the coordinates of similar interlayers to be revealed with a sufficient accuracy.

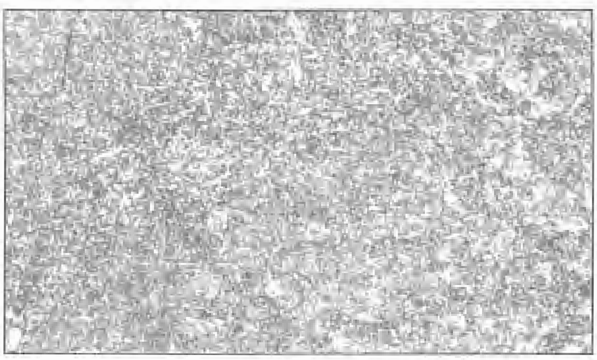

Figure 5. Microstructure of HAZ fusion zone. Automatic welding in CO_2 at recommended conditions, steel 15Kh1M1F (×100) (reduced by 0.80).

To prevent the formation of interlayers in the region of fusion, in case when chemical composition of the parent and weld metal is different, the edges of the parent metal should be minimum melted and welding should be done under the moderate conditions [12]. At such conditions the probability of appearance of such defects as lack of fusion at the gap walls may increase in thick-walled welded joints.

It was experimentally established that at automatic CO_2 welding the bead layout in 1 – 2 layers should be done at heat input of 1.5 MJ/m (I_w = = 350 A, v_w = 20 m/h; in 3 – 4 layers — at 1.2 MJ/m (I_w = 300 A, v_w = 20 m/h); in 5 – 6 layers — at 1.6 MJ/m (I_w = 380 A, v_w = = 25 m/h).

Homogeneity of structure (Figure 5) provides the correspondence of mechanical properties (Figure 2) to the requirements of SD. Values *KCU* with a notch in the fusion region are 55 – 56 J/cm^2 that corresponds to the requirements of SD. Values of heat input, coordinated with modelling, can be used both for a manual and mechanized welding.

Deviation of heat input values in welding from the estimated values by an upper limit (i.e. its exceeding) causes not only formation of similar interlayers at the fusion region and their corresponding increase, but also the formation of a coarse-grained structure in the region of overheating, increase in tendency to weakening the structure of the region of a partial recrystallization of HAZ.

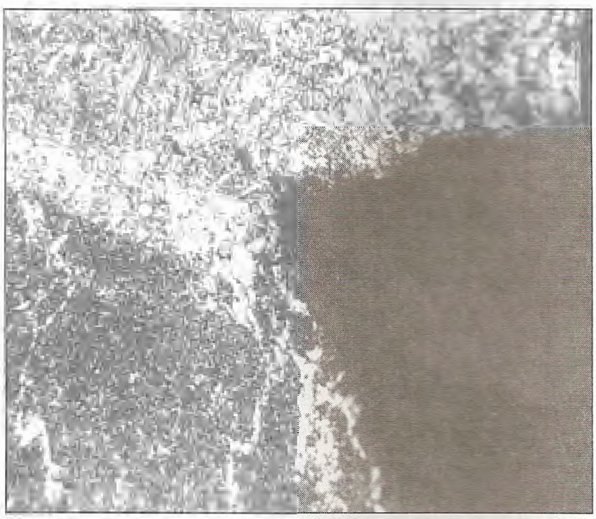

Figure 6. Microstructure at the region of fracture, running on «soft»interlayer in the fusion region. Welded butt of the steam pipeline, steel 12Kh1M1F, manual arc welding at conventional conditions (×100) (reduced by 0.75).

For comparison, the width of fusion region in welding under the conditions corresponding to the data of modelling is approximately 0.1 – 0.2 mm, while in welding under the conventional conditions it is by 15 – 20 % larger. It is known that brittle high-temperature fractures in «soft» interlayer, including that of the fusion region, are the main type of failures of welded joints of Cr–Mo–V steels in steam power plants (Figure 6) [1, 10]. Crack resistance is here additionally reduced due to the pre-sence of alternating dynamic stresses caused by increase in intensity of starts-stops of the power equipment. The allowable short-time overheatings in service of welded joints, for example of steel 12Kh1M1F (violation of requirements of SD) are characterized by the failure, mainly in the fusion region where the «soft» interlayers are located. Therefore, the prevention of formation of these interlayers is actual. To reach the goal it is necessary to produce an optimum initial structure of the welded joints by modelling the temperature conditions using the known data of methodological fundamentals.

The initial structure and properties of metal of the regions of overheating and partial recrystallization of HAZ, predicted from the results of modelling, should be considered separately. The further steps for prediction of producing the optimum structure and properties of the welded joints are seemed rational taking into account their heat-resistance, thus increasing the service life of the welded joints above 200000 h.

It should be noted in conclusion that the welding of Cr–Mo–V pearlitic steels with values of heat input obtained from data of modelling the temperature conditions with a keeping of SD requirements can prevent the formation of local «soft» interlayers in weld metal and at the fusion regions of HAZ, and also increase the short-time mechanical properties of the welded joints.

REFERENCES

1. Khromchenko, F.A. (1982) *Reliability of welded joints of pipes, boilers and steam pipelines*. Moscow: Energoizdat.
2. Zemzin, V.N., Shron, R.Z. (1978) *Heat treatment and properties of welded joints*. Leningrad: Mashinostroyeniye.
3. Krutasova, E.I. (1981) *Reliability of metal of power equipment*. Moscow: Energoizdat.
4. Pridantsev, M.V., Lanskaya, K.A. (1959) *Steels for boiler construction*. Moscow: Metallurgizdat.
5. Dmitrik, V.V. (1998) Method of determination of temperature conditions in weld pool melt. *Svarochnoye Proizvodstvo*, **8**, 19 – 23.
6. Dmitrik, V.V. (1999) Development of approximations of solutions of mating heat problems of arc welding with meeting all boundary conditions. *Novyye Resheniya v Sovr. Teknologiyakh*, **47**, 60 – 63
7. Dmitrik, V.V. (1999) Development of method of determination of temperature conditions of pool melt. *Izv. Vuzov*, **1**, 76 – 80.
8. (1982) *Recommened technical documents on welding, heat treatment and control of pipe systems of bilers and pipelines in site and repair of equipment of heat power stations*. Moscow: Energoizdat.
9. (1991) *Equipment and pipelines of nuclear power plants. Welding and surfacing. Main statements*. Moscow: Energoatomizdat.
10. (1981) *Analysis of damaged operating welded joints of steam pipelines of pearlitic heat-resistant steels*. Recommendations. Leningrad.
11. Reshetov, A.L., Klykov, N.A. (1978) Notch sensitivity of welded joints with soft interlayers. *Avtomaticheskaya Svarka*, **4**, 33 – 35.
12. Gotalsky, Yu.N. (1994) Problem of welding of quenching steels and known methods of its solution. *Ibid.*, 4, 36 – 40.
13. Grabin, V.F. (1982) *Metals Science of fusion welding*. Kiev: Naukova Dumka.
14. Kireev, V.A. (1969) *Short course of physical chemistry*.- Moscow: Khimiya.

FEATURES OF THE TECHNOLOGY OF ULTRASONIC WELDING OF AXIALLY SYMMETRICAL POLYETHYLENE CONTAINERS

N.P. NESTERENKO
The E.O. Paton Electric Welding Institute, NASU, Kyiv, Ukraine

ABSTRACT

The influence of modes of ultrasonic welding and methods of introducing mechanical vibrations into the weld zone on the quality of welded joints produced in sealing of polyethylene containers is considered. It is shown that with the decrease of the static compression force in the forging stage and of welding time the welded joint quality is improved at the expense of a more uniform morphology, absence of defects or texture in the weld zone. A new welding cycle and the appropriate schematic of dosing the energy of the introduced mechanical vibrations are proposed. Recommendations are issued on industrial use of the developed technology.

Key words: *ultrasonic welding of polyethylene, welding zone, methods of oscillations application, wave guide, wave guide oscillation amplitude, working frequency, piezoelectric transducer, upsetting, forging, working cycle.*

Ultrasonic welding (USW) of polyethylene is widely applied in fabrication of tanks, containers, pipes used for sealing the foods or household chemicals, as well as for storage of special-purpose liquid and powdered materials [1]. Contamination of the welding zone and presence of the product being packed into the container, make specific requirements of the USW process and, as a rule, lead to lowering of the welded joint quality.

This study was devoted to investigation of the technological features of pressure USW of parts of axially symmetrical containers of polyethylene of grade 158-10 (GOST 16337–85). In this case an integrated study was conducted of the influence of the wave guide oscillation amplitude, welding force and welding time on the welded joint quality, variants of applying ultrasonic oscillations (USO) to the welding zone were investigated and the optimal dimensions and shape of the surfaces being welded have been determined. This was the basis for development of an effective schematics of the process control.

The items being welded (Figure 1) consisted on a cover and case of $20\cdot10^{-3}$ m diameter and $4\cdot10^{-3}$ m height with the wall thickness of $1.1\cdot10^{-3}$ m. The containers are designed for storage and further use of easily inflammable granular substances. The initial requirements to this item assume its output in large quantities, presence of dust on surfaces being welded, localisation of the heating zone, weld tightness, correspondence of the finished item to strictly specified dimensions, as well as safety of the assembly process.

Several types of containers differing in the shape and dimensions of the surfaces being welded, have been manufactured for performance of technological work. This permitted investigation of the possibilities of welded joints production with different

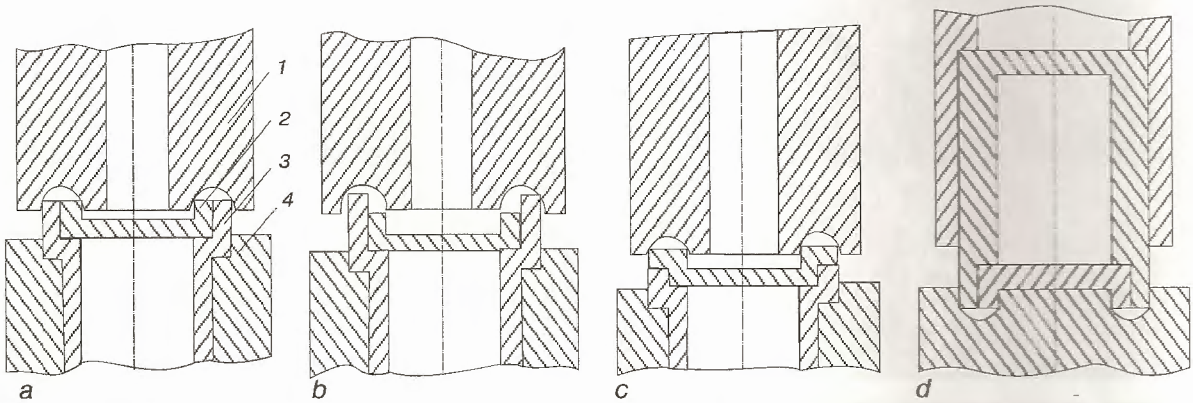

Figure 1. Joint geometry in container USW: *a* — from the side of the cover; *b* — with a greater protrusion of the case; *c* — in the near field; *d* — on the active support; *1* — wave guide; *2* — cover; *3* — case; *4* — support.

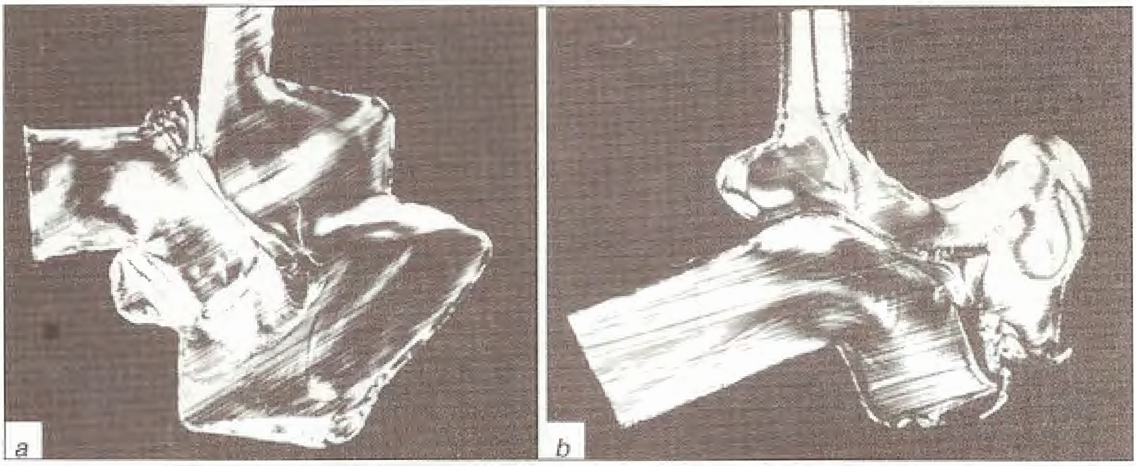

Figure 2. Zone of container weld in different welding modes: *a* — A = 40 μm; F_{com} = 120 N; t_w = 0.7 s; t_f = 0.5 s; *b* — A = = 35 μm; F_{com} = 120 N; t_w = 0.5 s; t_f = 0.4 s (×40) (reduced by 0.67).

variants of application of USO to the parts being welded: from the side of the cover (Figure 1, *a* – *c*) and from the side of the container casing (Figure 1, *d*). In this case the latter variant envisaged the possibility of welding both on an active and on a passive support.

Container welding was conducted at frequency f = 20 kHz. The other parameters of the welding mode were varied in the following ranges: amplitude of wave guide oscillation A = = $(10 - 45)\cdot10^{-6}$ m, static compressive force F_{com} = 100 – 600 N; welding time t_w = 0.5 – 5.0 s; forging time t_f = 0.1 – 3.0 s. Control of the welded joint quality was conducted in two stages: visual inspection of the weld and subsequent plastic graphical studies.

In the first variant (Figure 1, *a*) the cover and the case of the container had a circular protrusion of $3\cdot10^{-3}$ m height. In order to form a semi-circular weld, the working surface of the wave guide had a circular groove with $2\cdot10^{-3}$ m edge radius. The results of the conducted process studies showed that for this geometry of the edges being welded the «welding caterpillar» can be formed with the following parameters of the welding mode: A = = $40\cdot10^{-6}$ m; F_{com} = 120 N; t_w = 0.7 s. However, plastic graphical studies pointed to the presence of the fusion line in the weld zone (Figure 2, *a*), this being an indication of poor welding, namely low strength properties, possibility of cracking, etc.

Figure 1, *b* shows the diagram of USW of a container with an increased height of the case collar. Here the height of the case collar was selected to be such that after the weld formation the volume of the molten polymer did not exceed the volume of the circular groove of the wave guide. The welding process proceeded as follows; switching on USO before the moment of the wave guide touching the collar; exposing to sound the parts being welded at a constant static force F_{com}; switching off USO; forging at static compressive force $F_f = F_{com}$. At $A = 30\cdot10^{-6}$ m; F_{com} = 100 N; t_w = 0.9 s; t_f = 0.4 s melt splashing beyond the weld formation zone is practically absent, and no thinning or deformation of the container cover proper, is found. However, the zone of the formed bead and the case wall show discontinuities arising as a result of the melt overheating and subsequent thermal destruction of the polymer. As to the values of strength and tightness, this weld met the initial requirements, but the dimensions of the welded items showed a scatter of about 20 %, this going outside the requirements made of the finished item. Therefore, in order to shorten the welding time and reduce the scatter of data on weld geometry, the classical sequence of the welding cycle was assumed (compression–sonic treatment–forging) [1]. Welding was performed in the near field with limitation of the residual thickness of the weld. The container cover had the geometry given in Figure 1, *c*. In the welded joints (Figure 2, *b*) the weld has a pronounced fusion line and a zone filled with the polymer melt splashes from the container outer side, and also is of an obviously defective nature. Increase of the intensity of USW modes improves the joint quality. As shown by plastic graphical studies, however, a directed flowing of the melt is found in the weld zone in this case, thus somewhat lowering its strength properties. More over, a pronounced thinning of the container cover in the heat-affected zone did not permit performance of full-scale tests of the item as a whole.

The use of an active support (Figure 1, *a*) and application of USO from the container case side did not yield positive results. The welded joints produced in different modes, had a great scatter of the weld geometry, and burns-through were found in the zone of the wave guide contact with the container case.

The performed work on the technology led to the following conclusion: the container design shown in Figure 1, *b*, is the optimal one for USW, and the compressive force and oscillation amplitude should have the values of 100 N and $30\cdot10^{-6}$ m,

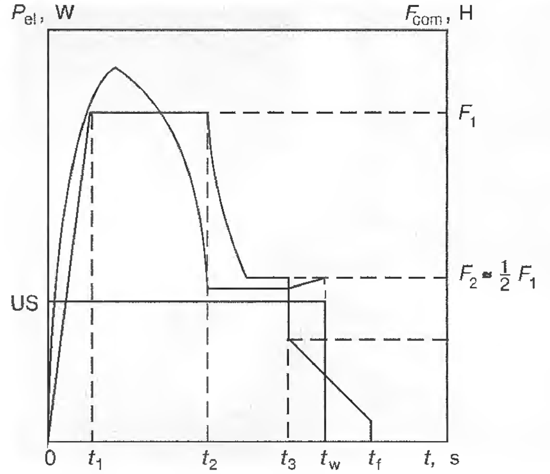

Figure 3. Working cycle of USW of polymer containers.

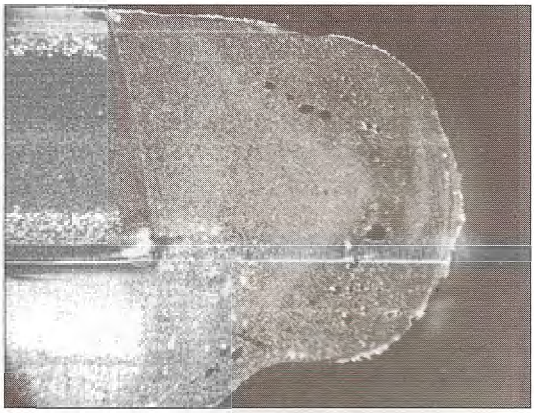

Figure 4. Zone of container weld with the following welding mode: A = 28 μm; F_{com} = 100 N; F_2 = 50 N (×40) (reduced by 0.67).

respectively. Here, in order to improve the welded joint quality at the expense of a more uniform morphology, absence of defects and texture in the interphase zones, the welding cycle should differ from the classical one, in particular at the stage of development of volume interactions in the weld zone and at the forging stage. More over, analysis of the derived results shows that the time dependencies of electric power $P_{el} = P_{el}(t)$ consumed by piezoelectric transducer during welding and polymer upsetting adequately represent the temperature and rheological processes proceeding in the welding zone. So, in particular, stabilisation of P_{el} corresponds to the start of the polymer transition into the plastic state, and the salient point on the material deformation curve corresponds to the start of an intensive flow of the melt in the welding zone. The predominant influence on the intensity of the thermomechanical processes is produced by the amplitude of the wave guide oscillations, and not the static F_{com}, this correlating well with the conclusions of the theoretical study [2]. Therefore, based on the results of the performed work on the technology of USW of polyethylene containers, a new welding cycle (Figure 3) was proposed whose essence is as follows.

At the moment of the acoustic head lowering ($t = 0$), USO are switched on, thus allowing the protruding collar of the container case to be melted off from the wave guide side practically just under the action of the dynamic forces. When time t_1 is achieved, this corresponding to complete melting of the collar, a static compressive force which is determined in advance, is applied to the items. At the moment t_2 of the start of stabilisation of P_{el}, $F_{com} = F_1$ drops to value F_2 which is determined experimentally. The welding bead forms during time $t = t_3 - t_2$. At the moment of time t_3 corresponding to the end of this process and the start of P_{el} rise, USO are switched off with a simultaneous lowering of the static force to F_2 value. Complete elimination of F_{com} occurs at the moment t_f of the weld zone achieving the assigned dimensions.

Deformation of the welding zone during the entire working cycle is measured and monitored by a differential-transformer transducer of linear displacement, while P_{el} consumed by the piezoelectric transducer during welding, by high-frequency wattmeter of A-410 type (Germany).

As shown by the performed study, practically for all the items from polyolefins with the above shape of the edges and the given operational sequence the following condition is satisfied: $F_2 = 1/2F_1$.

The welded joints produced during performance of the above working cycle, by their parameters have a repeatability not lower than 98 %. Optical microscopy of the weld zone (Figure 4) does not reveal any fusion line, although at the amplitude $A = 28 \cdot 10^{-6}$ m its surface layers can develop small cavities not influencing the tightness or strength of the joint.

The following modes are recommended, in order to provide the maximal productivity and the required strength and tightness: $f = (20 \pm 1.6)$ kHz; $F_1 = 100$ N; $F_2 = 50$ N with weld upsetting of $2 \cdot 10^{-3}$ m. With this method of USW control, the welding time is determined automatically, in keeping with the control criterion proposed above, and is in the range of 0.8 to 1.2 s. Therefore, the developed USW technology provides tight joints with the weld strength not lower than 70 % of the base material strength, with 98 % yield of sound items. In this connection, it has been accepted for introduction into pilot production.

REFERENCES

1. Volkov, S.S., Chernyak, B.Ya. (1986) *Plastics welding by ultrasound*. Moscow: Khimia.
2. Senchenkov, I.K., Chervinko, O.P., Nesterenko, N.P. (1991) Mathematical simulation of thermal vibration processes in technological systems for USW of plastics. In: *Abstr. of pap. of III All-Union Conf. on Mechanics of Inhomogeneous Structures,* Lvov, 1991. Lvov.

A NEW APPROACH TO DESIGN OF THE ELECTRODE WIRE FEED MECHANISM

V.A. LEBEDEV and **V.G. PICHAK**
The E.O. Paton Electric Welding Institute, NASU, Kyiv, Ukraine

ABSTRACT

The reduction gear mechanisms of electrode wire feed with roller motors, widely used in mechanized arc welding equipment, are analyzed. It is shown that with the increase of the feed roller diameter the values of tractive characteristics of the mechanism become higher, service life is extended and losses in the roller feed unit are reduced. A design of the feed roller is given characterized by a unrestrained mounting of the feeding element on the driving element. This provides the invariance of the electrode wire feed rate to its diameter, fast mounting and dismantling of the feed roller in the case of its replacement.

Key words: *mechanised arc welding, electrode wire, feed mechanism, feed rollers, design, dimensions, effectiveness.*

The mechanisms of electrode wire feed, incorporating an electric motor, speed-reducing gear, feed and pressure rollers, are extensively used in the majority of designs of mechanised arc welding equipment for various purposes. They must fulfil their functions with a high degree of accuracy, should be simple in design and adaptable to mass production. The propeller of the electrode wire in them is the feed roller — pressure roller pair. Such a type of propeller is quite versatile in terms of the possibilities which can be implemented in it, just by changing the profile of the surface interacting with the fed electrode wire. This concerns the feed rollers to a greater degree.

Study of the patent and technical literature [1, 2] enables analysis of the engineering solutions in terms of design of both the feed and the pressure rollers. Their diversity is great and the main ones are aimed at solving the following problems:

maximal adhesion of the rollers to the electrode wire with its minimal deformation;

feed of electrode wires of different diameters;

roller wear resistance;

fast removal and mounting of the rollers for their readjustment or replacement.

These tasks can be fulfilled in different ways, namely by special profiling of the rollers by making grooves of various shape, making cuts of different orientation, making rollers in the form of composite elements, synchronising the rotation of the feed and pressure roller using additional gears or making rollers in the form of gears with special profiling of the roller contact surface.

It is obvious that the roller design largely determines its pulling characteristics. Detailed analysis of different types of rollers is given in [3]. It shows, based on experimental studies of the pulling characteristics of rollers of different designs, different types and diameters of electrode wires, as well as different rates of their feed, that for any conditions the dependence:

$$F_{\text{pul}} = f\,(D_{\text{f.r}}),$$

where F_{pul} is the pulling force of the rollers; $D_{\text{f.r}}$ is the diameter of the feed roller, is a rising one, i.e. the pulling force increases with the roller diameter.

In our opinion, this phenomenon has the following explanation. Let us consider Figure 1, which shows the relative position of one of the rollers and the electrode wire fed by it. The dependence of the contact area length l_{c} on roller diameter $D_{\text{f.r}}$ can be determined from the geometrical constructions in this Figure, in the following form:

$$l_{\text{c}} = 2\sqrt{D_{\text{f.r}}\,\lambda - \lambda^2}, \tag{1}$$

where λ is the plastic or elastic deformation of electrode wire.

It follows from equation (1) that increase of the roller diameter leads to an increase of the contact spot as a result of the above roller deforming the electrode wire, and, therefore, to a greater valua of the coefficient of their adhesion to each other. The result of this process is an increase in the pulling capacity of the feed unit, which is enhanced still further by special profiling of the roller, as well as by its knurling. This is evident, provided the wire deformation λ remains constant irrespective of the roller diameter. Note that in order to provide λ stability, the force of electrode wire pressing should be increased with the roller diameter, in keeping with the data of [4] under the condition of elastic deformations:

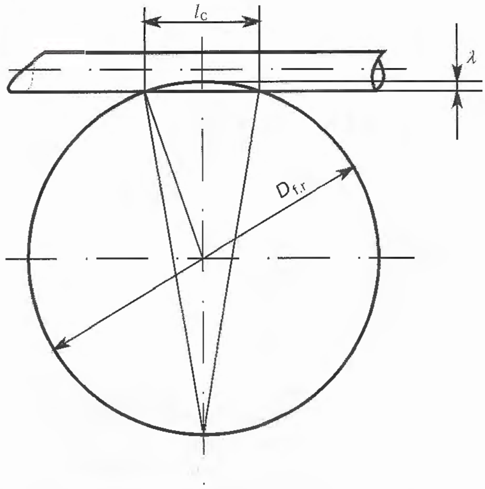

Figure 1. Relative position of the feed roller and the electrode wire.

$$\lambda = \alpha \sqrt[3]{\frac{P}{2\nu} \frac{R_{f.r} + R_e}{R_{f.r}\, R_e}}, \qquad (2)$$

where $R_{f.r}$ and R_e are radii of the feed roller and the electrode wire, respectively; P is the pressure force; α is the value dependent on $R_{f.r}/R_e$ ratio and slightly decreasing with the increase of the above ratio; ν is the coefficient allowing for the elastic deformations and determined in the form of

$$\nu = \frac{E_1}{1 - \mu_1} + \frac{E_2}{1 - \mu_2},$$

where E_1, E_2 and μ_1, μ_2 are the modulus of elasticity and Poisson's ratio for the feed roller and the electrode wire, respectively.

Considering that for the actual values of $D_{f.r} > \lambda > \lambda R_e$, let us substitute expression (2) into equation (1) to have the following dependence:

$$l_c = 2\sqrt{D_{f.r}\, \alpha \sqrt{P}/\nu D_e}, \qquad (3)$$

where D_e is the electrode wire diameter.

Analysis of equation (3) shows that the length of the contact area depends more on the feed roller diameter, than on the pressure force or electrode wire diameter. This equation gives just an approximate description of the actual phenomena in the contact zone of the electrode wire and the feed roller, it, however, can be used for evaluations. The above said indicates that it is rational to increase the feed roller diameter, in order to improve the pulling characteristics of the roller mechanism of electrode wire feed with its minimal deformation. Note that the electrode wire deformation is accompanied by certain energy consumption which can be attributed to hysteresis losses. These losses necessitate an increase in the power of the driving electric motor in proportion to the expression given in reference book [5]:

$$T_r = P\left(\frac{f_1 d + 2f_2}{D_{p.r}} + \frac{2f_2}{D_{f.r}}\right) k_1 k_2, \qquad (4)$$

where T_r are the losses in the roller feed unit; $D_{p.r}$ is the pressure roller diameter; f_1 is the friction coefficient in the pressure roller bearing; d is the average diameter of the bearing; f_2 is the coefficient of rolling friction of the feed roller over the electrode wire; k_1 and k_2 are the coefficients allowing for the type and accuracy of the roller manufacture, respectively.

Analysis of equation (4) leads to the conclusion that losses in the roller feed unit also depend on the rollers diameter, these losses becoming smaller with the increase of the diameter of, for instance, the feed roller.

Thus, increase of the diameters of the feed rollers allows an essential change in the technical and service parameters, namely

improvement of the pulling characteristics;

reduction of the losses in the roller units with the appropriate reduction of power of the driving electric motor;

extension of the service life as result of elongation of the roller working surface contacting the electrode wire being fed.

However, it is rather difficult to implement the required increase of the feed roller diameter and when a great increase is necessary, it is practically impossible. The cause for that is the existing approach to development and design of the reduction gear feed units with roller propellers of electrode wire.

Reference [6] gives the procedure of designing reduction gear feed units from which it follows that with the selected drive electric motor with a certain nominal frequency n_{nom} of its shaft rotation, as well as with the specified upper value of the electrode wire feed rate $v_{e\,max}$, the reduction gear transfer ratio i is determined as

$$i = \frac{60 D_{f.r} n_{nom}}{1000 v_{e\,max}}. \qquad (5)$$

From expression (5) it follows that increase of the feed roller diameter inevitably leads to the rise of the transfer ratio of the reduction gear, thus promoting an increase of the number of kinematic pairs or of its overall dimensions, or reduction of modules of kinematic gear pairs both individually and in different combinations. All this is in the way of improvement of the reduction gear efficiency, lowers its reliability or increases the material content. With different variants of increase of the reduction gear transfer ratio, its different drawbacks can also be manifested. It is evident that with such a procedure of design of the roller reduction gear feed units, an arbitrary change of the feed roller diameter is impossible, while being obviously rational.

The impossibility of an arbitrary increase of the feed roller diameter is due to the fact that the feed roller, reduction gear and electric motor are rigidly coupled to each other, and with the design values of the transfer ratio, any change in the feed roller diameter invariably leads to a change in the electrode wire feed rate. This change can be compensated, for instance, by widening the range of adjustment of the feed unit electric drive, this making necessary the use of regulators with unjustified high values of the above adjustment range. More over, application of regulators with a wide range of adjustment does not provide a solution for all the problems concerning optimisation of the design parameters of the rollers for feeding electrode wires of a broad range of diameters, designs and materials, as well as the problems related to extension of the roller service life compared to the values given in GOST 18130–79 and being equal to 50 h.

The Experimental Design Technological Bureau of the E.O. Paton Electric Welding Institute suggested a new approach to the problem of design of the roller mechanism of electrode wire feed, which envisages a division of the feed roller in terms of design, into two main functional objects, namely drive roller mounted on the reduction gear output shaft and feed roller freely mounted on the drive roller surface.

The design of the proposed engineering solution is schematically shown in Figure 2. Drive roller *1* made in the form of a gear is rigidly mounted on the output shaft of the reduction gear. Feed roller *2* is freely mounted on it, the roller also made in the form of a gear but with the inner gearing which moves into engagement with the gearing of roller *1*. Pressure roller *3* presses electrode wire *4* to feed roller *2*.

Rotation is transferred from drive roller *1* through the gearing to feed roller *2* which, being clamped between pressure roller *3* and electrode wire *4* is also imparted rotation and moves the electrode wire. The axis of rotation of feed roller *2* does not coincide with the axis of rotation of drive roller *1* and is not mechanically coupled with anything, which makes the difference between the proposed mechanism and those traditionally used with rigid coupling of all the axes of rotation.

It is obvious that the rate of electrode wire feed in the mechanism being considered, is determined by the frequency of rotation, diameter of the drive roller-gear *1* and is not associated with the feed roller diameter *2*. The feed roller rotation frequency $n_{f.r}$ depends on the ratio of $D_{f.r}$ and D_{dr} and is given as

$$n_{f.r} = \frac{n_{dr} D_{dr}}{D_{f.r}},$$

where n_{dr} is the frequency of drive roller rotation.

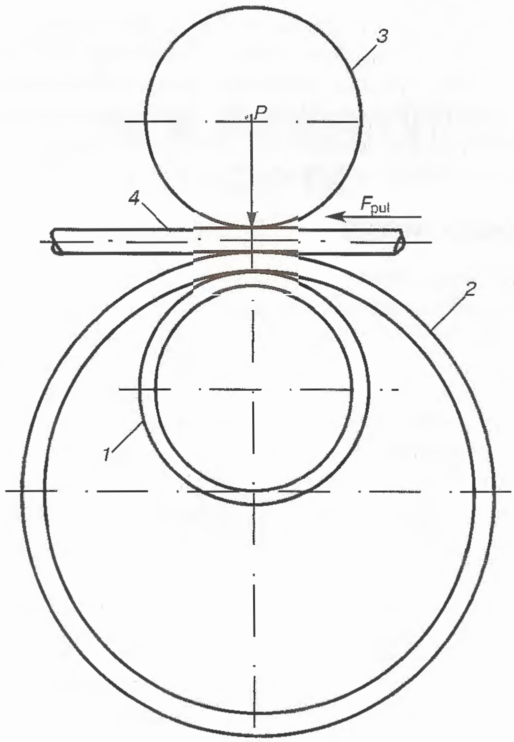

Figure 2. Diagram of a new roller mechanism of electrode wire feed.

Note that with the change of the feed roller diameter in the design under consideration, the moment of resistance to feed, transferred to the drive electric motor remains the same and minimal (dependent only on the drive roller diameter and thickness of the ring which forms the feed roller).

In addition to the above advantages of feed rollers of increased diameters, still another one should be noted, namely the ability of a fast removal and mounting during replacement.

The mechanism with the free feed roller can have different designs. So, the feed roller proper is made of two main parts, namely gear with inner gearing and rigidly coupled to it removable rim with the surface suitable for electrode wire feed.

The possible axial offset of the feed roller can be provided by several engineering solutions. The simplest one are the limiting washers, another consists in making the gearing with the protrusions and recesses, thus providing its self-adjustment and self-locking through axial offset of the feed roller.

The most effective engineering solution is an assembly for pulsed feed mechanisms based on a quasi-wave transducer [7], where significant accelerations in the pulsed movement arise and a reliable transfer of the pulling forces from the feed roller to the electrode wire is required.

When experimenting with the free feed rollers, their several designs have been made and tested. One of the variants of the pair of drive and pressure rollers of 24 and 78 mm diameter, respectively, and with inner gearing, was mounted in a modified semi-automatic machine PSh107V for feeding flux-cored and aluminium wires with a certain orientation of the grooves profiling on the roller feed element. In operational trials of such a design the rollers ran for more than 240 h, providing a high degree of feed reliability.

CONCLUSIONS

1. Pulling forces, fatigue life, and losses in roller feed unit, essentially depend on the feed roller diameter, besides other design parameters. With the increase of the feed roller diameter, its pulling characteristics and service life are essentially improved, while the losses are reduced.

2. A design of the feed roller is proposed, freely mounted on the drive part, which interacts with it by means of a gearing, and provides the invariance of the electrode wire feed rate to the diameter of the above feed roller.

3. The new design of the feed roller with the free mounting predetermines such procedures of selection and calculation of the roller reduction gear feed unit in which just the parameters of the roller drive part need to be taken into account.

REFERENCES

1. Chvertko, A.I., Belfor, M.G., Paton, V.E. *et al.* (1975) Directions of development of electrode wire feed mechanisms in up-to-date arc welding machines. *Avtomaticheskaya Svarka*, **10**, 56 – 60.
2. Lebedev, V.A., Nikitenko, V.P. (1983) Promising trends in design of electrode wire feed mechanisms (Review). *Ibid.*, **7**, 61 – 69.
3. Belfor, M.G., Livinsky, V.P., Paton, V.E. *et al.* (1971) Roller devices for electrode feed in the units for arc and slag welding. *Ibid.*, **12**, 29 – 35.
4. Pisarenko, G.S., Agarev, V.G., Kvitka, A.L. *et al.* (1963) *Resistance of materials*. Kiev: Gostekhizdat UkrSSR.
5. (1986) *Equipment for arc welding*. Reference book. Ed. by V.V. Smirnov. Leningrad: Energoatomizdat.
6. Chvertko, A.I., Paton, V.E., Timchenko, V.A. (1981) *Equipment for mechanised arc welding and surfacing*. Moscow: Mashinostroyeniye.
7. Lebedev, V.A., Moshkin, V.F., Pichak, V.G. (1996) New mechanisms for pulsed feed of electrode wire. *Avtomaticheskaya Svarka*, **5**, 39 – 44.

INVESTIGATION OF THE INFLUENCE OF GRAVITY ON THE COMPOSITION OF COATINGS FROM BINARY Ag–Cu ALLOYS*

E.S. LUKASH[1], **V.F. SHULYM**[1], **G.M. GRIGORENKO**[1], **O.D. SMIYAN**[1] and **L.O. NEZNAMOVA**[2]
[1]The Paton Electric Welding Institute, NASU, Kyiv, Ukraine
[2]RSC Energia, Moscow, Russia

ABSTRACT

The method of Auger-spectroscopy was used to study the composition of coatings of Al–Cu alloys produced under different gravity conditions. Some features of formation of coatings from binary alloys under zero gravity are considered. The results of metallographic investigations of the structure of the alloys remnants after evaporation in space and on the Earth are given.

Key words: *alloy, coating, zero gravity, gravity, metallurgical investigations.*

The experiments on deposition in space of thin films of braze metals based on Ag–Cu alloys on different substrates, conducted in the «Isparitel» unit in 1981 demonstrated, alongside important applied results, also some laws which are of essential scientific interest, for instance, the anomalous nature of evaporation of binary alloys at microgravity [1]. During the following years these experiments were carried on in «Isparitel-M» unit. Evaporation of binary alloys with markedly different vapour pressure of the components on the Earth is accompanied by a continuous change of the coating composition compared to the initial alloy [2 – 4]. Known are the theoretical and experimental dependencies of the content of components in the coating on the time of evaporation of the following alloys: Ag–Cu; Sn–Cu; Sn–Pb; Sn–Ag; Ag–Al [5]; Ni–Cr [6]; Al–Mg [7]. Nonetheless, a number of methods are used in the technology of production of coatings from binary alloys, which allow making thin films of the specified relatively stable composition, namely «flash» evaporation [8], evaporation from different sources [9, 10], from the «solid» state [11]. However, the disadvantages inherent to the above methods often lead to deterioration of the film quality. Therefore, the problem of production of coatings from binary alloys with preservation of the initial material composition is still urgent.

The paper presents the results of investigation of the composition of coatings produced in evaporation of Ag–Cu alloy in space and on the Earth. The fact that diffusion is the main mechanism of mass transfer at zero gravity, allows the assumption to be made that the process of binary alloy evaporation from the molten state in space is similar to evaporation from the «solid» state on the Earth. In the case if this assumption is confirmed, broad capabilities would be opened up for production of coatings from binary alloys with preservation of the initial material composition. This can turn out to be especially important for the alloys in which one of the components is present in an extremely small amount, whereas its vapour pressure is markedly different from the vapour pressure of the main component.

Space experiments and their ground analogs on evaporation of Cu–26 at.% Ag and Cu–10 at.% Ag alloys were conducted in the «Isparitel-M» unit in the spring of 1984 by a procedure described in [12]. Glass (25.0 × 25.0 × 0.5 mm) and titanium (60.0 × × 80.0 × 0.2 mm) substrates were used. The substrate surface was thoroughly degreased prior to coating deposition. It should be noted that the evaporation process was of a discrete nature. Coatings were successively deposited from one crucible onto 12 substrates mounted on a drum-like sample holder. The coating on each of the substrates was produced after preheating of the evaporation material (with the closed shutter). The exposure was from 40 to 180 s in different periods of coating deposition. Each of the considered alloys was almost completely evaporated from the crucibles. The thickness of the produced coatings was measured in the interference microscope MII-4. Coatings on glass substrates were used for these purposes. The deposition rate during the entire process was evaluated by the results of thickness measurement, tak-

* Published in: *Problems of space technology of metals*. Kiev: PWI, 1986, pp. 22 – 28.

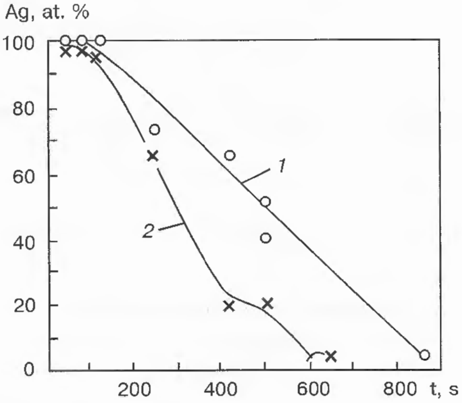

Figure 1. Dependence of silver content in the coating on the time of evaporation of Cu–26 at.% Ag alloy: *1* — on the Earth; *2* — in space.

ing into account the time of exposure. The coating thickness was from 30 up to 200 nm. The composition of the produced coatings was determined by the Auger-spectroscopy method. It is the only suitable method from the known compositional analysis methods, as it has the information depth of 2 to 5 nm (depending on the primary electron energy). LAS-2000 unit of «Riber» company for three-dimensional surface analysis with Auger-microprobe of cylindrical mirror type was used. Before the start of analysis, the sample surface was cleaned from adsorbates and surface contamination by a special low current CI-10 ion gun (ion energy of 1 keV, etching duration of 10 min) in the pre-chamber. During this time 0.5 to 1 nm layer was removed from the coating surface. Then the sample was moved into the analysis chamber with the pressure of the atmosphere of $1.3\cdot10^{-7}$ to $3.9\cdot10^{-8}$ Pa. The coating was etched off using a more powerful CI-40 ion gun which operated in the scanning mode. 50 nm layer was etched off in 10 min. Information which was derived during investigations was plotted by XY-recorder in the form of the energy spectrum. The measurement accuracy was 10 %. Metallographic investigations of the remnants after evaporation of Cu–26 at.% Ag and Cu–10 at.% Ag alloys were conducted in «Neofot-2» microscope on microsections prepared by the universally accepted procedures. VUP-4 unit was used to reveal the structure in the following mode of cathode etching: I = 10 mA; U = 5 kV; $P = 1.3\cdot10^{-2}$ Pa; t = = 20 – 35 min. The elemental composition of the remnants after the alloys evaporation, was determined in X-ray microanalyser «Cameca».

Change of silver content (and copper content, respectively) in the coatings during evaporation of Cu–26 at.% Ag alloy is illustrated by Figure 1. It can be seen that in evaporation of Cu–26 at.% Ag alloy on the Earth (Figure 1, curve *1*) first silver intensively evaporates, whose vapour pressure is by an order of magnitude higher, than that of the copper vapours at the same temperature. Under these conditions, the main cause for mass transfer is the temperature convection, that is why continuous rather fast enrichment of the surface layer with the highly volatile component (silver) takes place. During evaporation, as follows from the Raoult law, a continuous change of the composition of the produced coatings is found. In this case, all the silver which was in the alloy, evaporated. X-ray analysis of the remnants of Cu–26 at.% Ag alloy after evaporation on the Earth, showed it to contain pure copper. This is confirmed by the results of metallographic investigations (Figure 2, *a*).

At zero gravity the process of material evaporation has its special features, as the mass transfer under these conditions is primarily determined by the thermocapillary and chemical convection, as well as diffusion. The first two processes have certain inertia in viscous liquids, their intensity is by several orders of magnitude lower, than that of the normal temperature convection, and as they are related to surface tension, they are active only in the zone immediately adjacent to the interphases. Their role in mass transfer at short exposures is so small that it can be neglected. The main cause for mass transfer in this case is diffusion, although this process also has considerable inertia. In evaporation of binary alloys at zero gravity, such a state can be in place when the evaporation rate of the more volatile component and the rate of diffusion of this

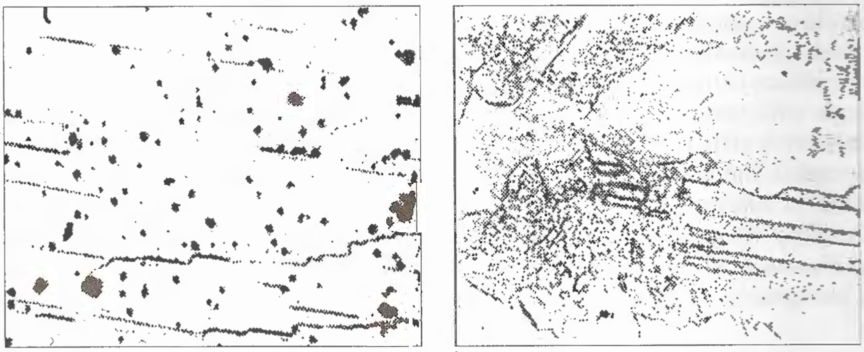

a b

Figure 2. Microstructure of the remnants of Cu–26 at.% Ag alloy after evaporation on the Earth (*a*) (×500) and in space (*b*) (×200).

component to the surface, balance each other. A steady-state condition will set in, in which the composition of the produced coatings will remain unchanged. This will occur at a certain and constant temperature of the alloy being evaporated. It is natural that in this case a plateau should be present in the plot of the dependence between the alloy component content and the evaporation time.

As was already mentioned, in order to solve the applied tasks, the duration of the substrates exposure to the vapour flow and the temperature of Ag–Cu alloy being evaporated, and, therefore, the rate of its evaporation, were varied during the experiments on coatings production in space and on the Earth. The alloy temperature in the crucible was changed from 1250 up to 1550 °C. That is why (Figure 1, curve *2*), it has been so far impossible to get experimental confirmation of the theoretical postulates, except for one short-term section when the alloy evaporation proceeded without any change in the composition. The influence of the discrete nature of the evaporation process on the anticipated result, could not be avoided.

However, analysis of the given results still allows tracing certain features of evaporation of the studied alloys at zero gravity. So, in determination of the layer-by-layer composition by the Auger-spectroscopy method, the following regularity was found. If copper is present in the coating, the surface is enriched in copper, and in the coatings produced in space the layer enriched with copper, is several times thicker. This is confirmed by the run of curves *1* and *2* in Figure 1. It can be seen that copper from Cu–26 at.% Ag alloy, starts evaporating in space earlier, than on the Earth (curve *2* falls more abruptly than curve *1*). In each point of curves *1* and *2* corresponding to a certain evaporation time, silver content in the space coatings is smaller, than in the ground ones, and that of copper is greater, respectively. In this connection, the results of evaluation of the evaporation rate of Cu–26 at.% Ag alloy at the same crucible temperature (approximately 1490 °C) in the space and ground experiments, are of interest (Figure 3). The form of

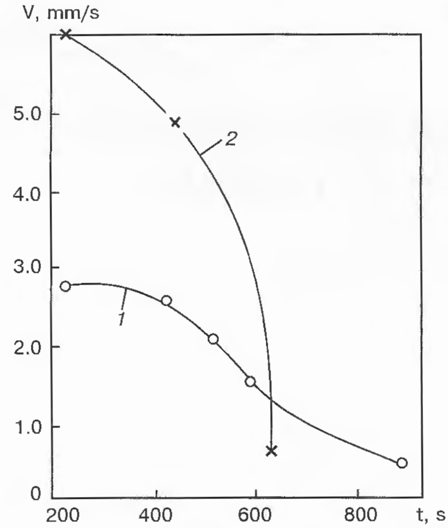

Figure 3. Change of evaporation rate of Cu–26 at.% Ag alloy during its evaporation under the terrestrial (*1*) and space (*2*) conditions in the same modes.

curves *1* and *2* shows that the less volatile component of the alloy, copper, makes a more significant contribution to the change of the evaporation rate in the space experiment. In the ground variant the alloy evaporation rate is determined by pure silver evaporation rate for a rather long time (see Figure 3, initial section of the curve). By absolute value the respective evaporation rates (see Figure 3) are higher in space, than on the Earth. Therefore, the same amount of the initial Cu–26 at.% Ag alloy evaporated faster in space (see Figure 1, curve *2*), than on the Earth (see Figure 1, curve *1*).

The curves of the dependence of silver content (and copper content, respectively) in the coatings of Cu–10 at.% Ag alloy produced in space and on the Earth are, on the whole, similar to the respective curves for Cu–26 at.% Ag alloy. Because of a small content of silver in the initial alloy, however, its evaporation rate is determined primarily by the low volatile component, that is copper. Therefore, in the remnants after evaporation of Cu–10 at.% Ag alloy in space and on the Earth (total evapo-

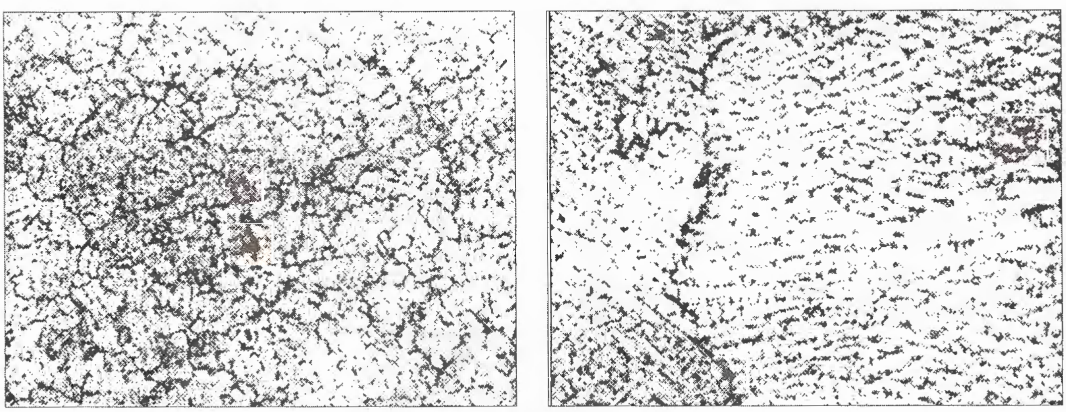

a *b*

Figure 4. Microstructure of the remnants of Cu–10 at.% Ag alloy after evaporation on the Earth (*a*) and in space (*b*) (×50).

ration time being the same as for Cu–26 at.% Ag alloy), the content of silver fractions by weight is 5 – 7 % (by the data of X-ray microprobe analysis). Also significant is the fact that in evaporation of Cu–10 at.% Ag alloy on the Earth the time of pure silver evaporation from it is longer than in a similar experiment for Cu–26 at.% Ag alloy. In evaporation of these alloys in space, the influence of the low volatile component, copper, is manifested in almost the same fashion. This results from the fact that the cause of mass transfer on the Earth is convection and in space it is diffusion. Note also the differences in the structure of the remnants after evaporation of the above alloys in space and on the Earth. Comparison of copper microstructures given in Figure 2, *a*, *b* shows that the structure of the metal solidified in space is more perfect. The etching pits are easily visible even with 200X magnification. It is known [13] that in solidification of binary alloys, the grains in the structure of the space samples have somewhat larger dimensions, compared to the structure in the ground samples. Comparison of microstructures of the remnants of Cu–10 at.% Ag alloy after evaporation on the Earth (Figure 4, *a*) and in space (Figure 4, *b*) confirms this conclusion.

In view of the above said, it is possible to make the conclusion that despite the preliminary nature of the performed investigations, they point to good prospects for further study of the influence of zero gravity on the process of binary alloy evaporation, both in terms of development of fundamental research and in terms of practical application.

REFERENCES

1. Lukash, E.S., Lapchinskii, V.F., Shulym, V.F. *et al.* (1985) Some results of analysis of the coating samples produced in space. In: *Problems of space technology of metals*. Proc. of 1st All-Union seminar. Kiev: Naukova Dumka.
2. Berry, R.W., Hall, P.M., Harris, M.T. *et al.* (1968) *Thin film technology*. New York: Norstard.
3. (1977) *Thin film technology*. Handbook. Ed. by L. Micella, P. Glag. Moscow: Sov. Radio.
4. (1976) *Epitaxial growth*. Ed. by J.W. Matthews. New York: Academic Press.
5. Saur, E., Unger, E. (1958) Spektralanalytische Untersuchung des Verdampfungsvorganges binaerer Legierungen. *Zeitschrift Naturforschung*, **13a**, 72 – 79.
6. Huijer, P., Langendam, W.T., Lely, J.A. (1963) Vacuum deposition of resistors. *Philips Techn.*, **24**, 144 – 149.
7. Boettcher, A. (1950) Ueber Herstellung und Aufbau aufgedampfter duenner Al–Ag und Al–Mg Schichten. *Z. Angew. Phys.*, **2**, 193 – 203.
8. Beckerman, M., Bullard, R.L. (1962) *Proc. of Electronic Compon. Conf., Washington*.
9. Mader, S. (1965) Metastable Alloy Films. *J. Vacuum Sci. Technol.*, **2**, 35 – 41.
10. Ostander, W.J., Lewis, C.W. (1962) Electrical properties of metal-dielectric film. In: *Trans. 8th Nat. Vac. Symp., Washington, 1961*. New York: Pergamon Press.
11. Shneider, M. (1959) *Techn. Mitt. PTT*, **465**, 470.
12. Shulym, V.F., Zagrebelny, A.A., Lapchinskii, V.F. *et al.* (1985) Hardware for evaporation of materials in space. In: *Problems of space technology of metals*. Proc. of 1st All-Union seminar. Kiev: Naukova Dumka.
13. Ivanov, L.I., Kubasov, V.P., Pimenov, V.N. *et al.* (1977) Melting of copper-aluminium alloy and aluminium powder at zero gravity. *FIKhOM*, **6**, 35 – 39.

STRUCTURE OF MARTENSITIC-FERRITIC STEELS AFTER SURFACE PLASMA HARDENING

A.V. TUGOLUKOV[1], O.N. KLYUCHNIK[1] and E.D. BUDYUK[2]
[1]Concern Stirol, Artemivsk, Ukraine
[2]Ukrainian State Chemical-Technological University, Dnipropetrovsk, Ukraine

ABSTRACT

Surface plasma treatment provides a fundamental increase in hardness of steel 20Kh17N2. This is achieved by varying power of the plasma jet and increasing its concentration. Metallography revealed three characteristic regions formed as a result of the plasma jet effect. An increase in the concentration of the heat flow affecting the sample surface causes a decrease in the hardened and transition zones, decrease in the amount of carbides in the bulk of the main phases and reduction in grain size.

Key words: *surface plasma hardening, plasma jet, hardness, martensitic and ferritic phases, carbides, hardened and transition zones.*

Failure in operation of such parts of chemical engineering equipment as pump shafts, half-couplings and rods is caused primarily by intensive cracking under dynamic and alternating thermomechanical loads, accompanied by wear and corrosion.

It is a known fact that the process of surface plasma hardening provides a substantial increase in wear resistance of parts and is characterized by a high practicability [1].

The purpose of this work is to investigate principles and peculiarities of structurization of martensitic-ferritic steels after plasma heating and quenching, avoiding surface melting. Experiments on treatment of steel samples were conducted using a plasma heat-hardening machine developed by the Ukrainian State Chemical-Technological University in collaboration with the Open Joint-Stock Company «Concern Stirol». The machine consists of a lathe of the 163 model, plasmatron with a vortex stabilization of the arc, which is equipped with replaceable nozzles to form plasma flows of different configurations across the plasma jet section, DC power supply (APR404), control panel, plasmatron manipulator, water pump, plasma gas and water feed systems, ventilation and wastewater disposal system.

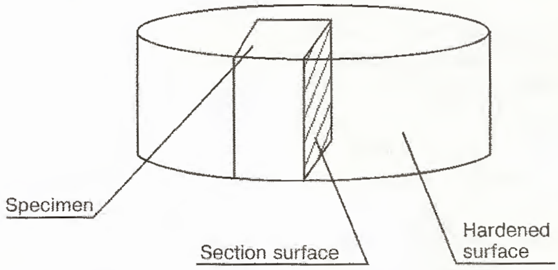

Figure 1. Schematic of cutting out and preparation of a metallography section.

Plasma treatment was done on round samples 85 mm in diameter and 350 mm long, made from steel 20Kh17N2 (0.20 % carbon, 0.52 % silicon, 1.83 % nickel, 0.18 % molybdenum, 0.36 % manganese, 17.03 % chromium and 0.01 % titanium). The travel speed of the jet relative to the surface treated was 7 mm/s. The plasmatron power consumption (w) was varied from 47.5 to 54.0 kW, and the distance (d) from the nozzle exit section to the surface treated was varied from 7 to 3 mm.

Specimens for metallographic investigations and evaluation of hardness were cut out as schematically shown in Figure 1. Height of the specimens was 20 mm. Hardness was measured using the TK-2M 2140TR hardness meter in compliance with GOST 9013–59. The metallography sections were prepared and investigated by commonly accepted procedures using the MIM-8 microscope.

Figure 2. Structure of the steel 20Kh17N2 sample before hardening (×600).

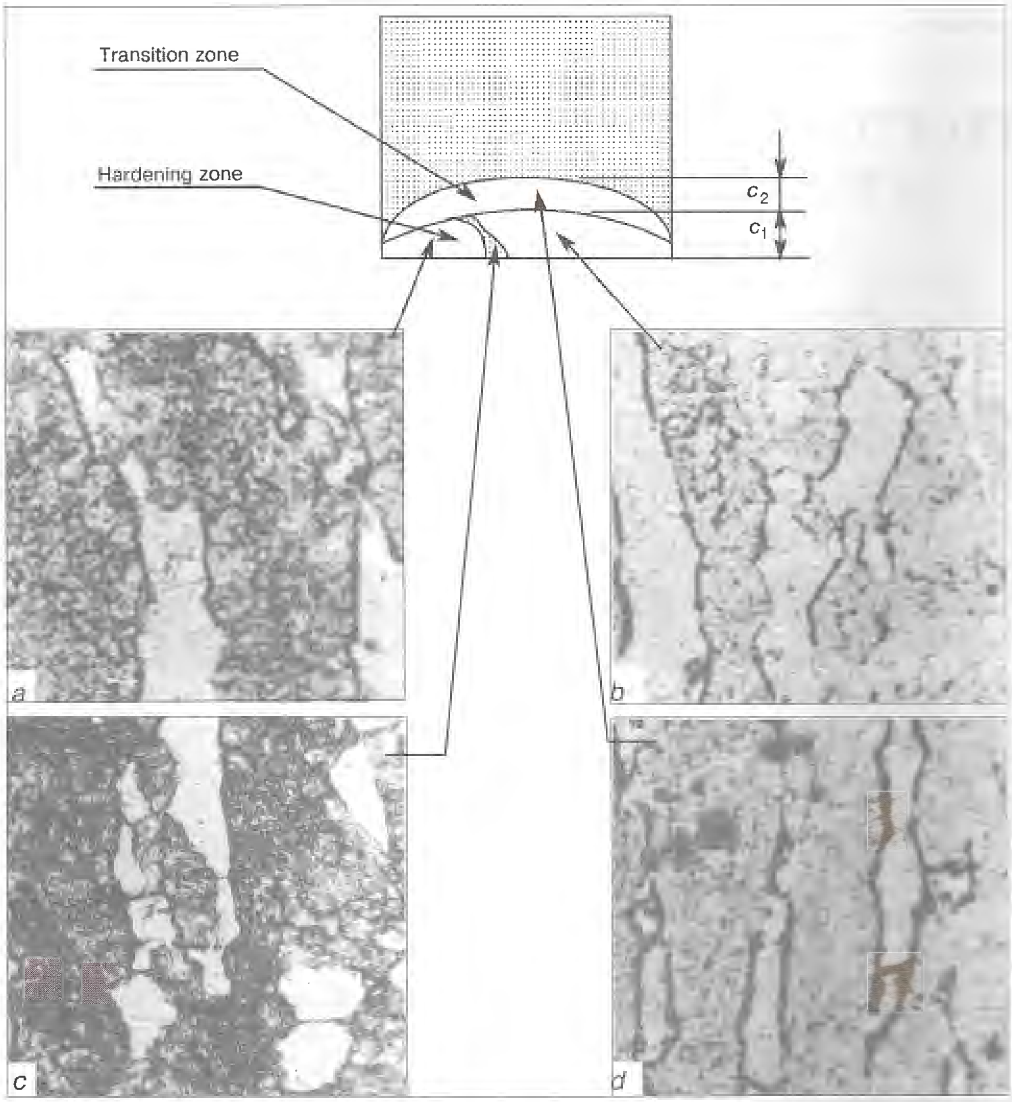

Figure 3. Microstructure of different zones in sample *1*: *a* — region I (decarburization zone); *b* — dark spot (hardening zone); *c* — region II (zone of insignificant tempering); *d* — transition zone (×600).

The structure was evaluated in compliance with GOST 8233–56.

It was found that hardness (*HRC*) of the hardened layer varied through the sample thickness from 35.3 to 44.0, hardness of the sample in the initial state being 22.3.

The transverse sections for metallography were taken from all samples. Etching the sections was done by the electrolytic method in a 10 % oxalic acid solution. The initial material was martensitic-ferritic steel with a ferrite (F) content of 15 – 20 vol. %. The martensitic (M) component was martensite corresponding to 7 – 8 points with the length of the needles equal to $L_m = 12 - 16$ μm (Figure 2). All the samples investigated had the hardened layer with a heterogeneous structure. Three characteristic regions differing in phase transformations were revealed in them. The central region was a dark spot 4 – 5 mm in diameter. The hardened and transition layers can be clearly seen in the sections after etching. All the samples had a decarburized subsurface layer 0.1 – 0.2 mm deep, which is seen near the section edge. Metal structure of the samples outside the hardening and transition zones remained unchanged. The length of the hardened and transition zones and their phase composition are shown in Figure 3 and given in the Table.

Plasma hardening was done without surface melting, but with subsequent overlapping the hardened zone. The machine was additionally tooled with a shut-off and quenching (for cooling the region immediately adjacent to the plasma spot) sprayers. The shut-off sprayer is intended to feed water for cooling the hardened strip to ensure heat insulation of the plasma jet within the heating zone from the hardened surface, avoid tempering and hardness decrease. Nevertheless, the presence of region II is a result of tempering the hardened zone by the peripheral part of the plasma jet in making the next pass. The dark spot is attributable to the

Structure of different regions in samples of steel 20Kh17N2 after surface plasma treatment

Regions and zones in samples (located as shown in Figure 3)	*Sample No. and characteristic of treatment process*			
	1	*2*	*3*	*4*
	w = 47.5 kW, d = 7 mm	*w = 54.0 kW, d = 7 mm*	*w = 54.0 kW, d = 5 mm*	*w = 54.0 kW, d = 7 mm*
	Structural characteristics			
I	C in the bulk of M and F (insignificant). N_c at the interface (5 – 6 p.). Amount and size of F is larger than in the initial structure. $F_{hard} > F_{init}$ and makes 25 – 30 % of area. Individual precipitates of δ-F	M + F + C (in the bulk of M and F). C at the M–F interface (1 – 2 p.). L_m = 12 – 16 μm. M (7 – 8 p.). F_{hard} = = F_{init}. No δ-F	M + F + C (individual precipitates in M and F). N_c at the M–F interface (5 – 6 p.). M (7 – 8 p.). L_m = 12 – 16 μm. F_{hard} = = F_{init}. No δ-F	M + F + C (individual inclusions in the bulk of M and F). N_c at the M–F interface (5 – 6 p.). M (6 – 7 p.). F_{hard} = F_{init}. No δ-F
Dark spot zone	F, δ-F and P (granular). δ-F – up to 40 % of F. C along the F boundaries (5 – 6 p.)	F + P (granular). C along the boundaries (5 – 6 p.). F_{hard} = F_{init}. No δ-F	F + P (granular). N_c at F (6 p.). $F_{hard} < F_{init}$. F_{hard} as δ-F	F + M + P (granular). P – minimum. No C along the F boundaries. F_{hard} = F_{init}. No δ-F
II	C in M and F (minimum). F ~ 25 – 30 % of area. C at M–F (3 – 4 p.). δ-F ~ 3 – 5 % F	M + F + C (in the bulk of M and F). F ~ 25 – 30 % of area. C at the M–F interface (3 – 4 p.). δ-F – individual grains. M–F	C in M (insignificant in F). N_c (3 – 4 p.). F_{hard} = = F_{init}. No δ-F	Minimum C in the bulk of F and M. No N_c. F_{hard} = F_{init}. No δ-F
Transition zone	M + F + C. M – fine needles (2 – 3 p.). L_m = = 2 – 4 μm. N_c along the interface (6 p.). No δ-F	M + F + C. M (7 – 8 p.). L_m = 12 – 16 μm. C (6 p.). F_{hard} = F_{init}. No δ-F	M + F + C. M (8 – 9 p.). L_m = 16 – 20 μm. C at the M–F interface (6 p.). F_{hard} = F_{init}. No δ-F	M + F + C. M (5 – 6 p.). L_m = 8 – 10 μm. N_c at the M–F interface (6 p.). F_{hard} = F_{init}. No δ-F
Length of the zones, mm				
hardened c_1	1.2	0.8	0.5	0.3
transition c_2	0.9	1.0	0.9	0.4

Notes: 1. Size of carbide network grains and length of needles of the martensitic component were determined from the scales and tables of GOST 8233–56. 2. Location of carbide inclusions in martensite was attributed to initial martensite needles. 3. Carbide network was located at the interface and along the grain boundaries. 4. Granular pearlite (P) is likely to be a product of tempering of martensite to temperatures close to A_{r1}; F_{init} and F_{hard} are the amount and size of ferrite in initial state and after hardening, respectfully.

effect of a maximum temperature on the sample surface. The results given show that for region I (subsequent passes do not cause its tempering) an increase in power input to the plasmatron and a decrease in distance to the surface enable size of the martensitic component and length of its needles to be decreased by preserving the amount and size of the ferritic component. Within the zone of the dark spot, an increased power concentration results in the formation of a structure which is characterized by the absence of the carbide network (N_c) along the grain boundary, which can be caused by the thermal cycling effect [2]. The increased power concentration in region II, which is a region with an insignificant tempering by the plasma jet, provides a minimum content of carbides (C) in the bulk of the main phases and grain sizes comparable with those in the initial state. Structure of the transition zone in sample *1* (with filling the plasma spot) is advantageous in that it is characterized by a fine-needle structure of martensite and a maximum development of the zone with this structure.

It can be concluded that plasma hardening results in a substantial increase in hardness of steel which is hard to treat by conventional volumetric quenching. It is likely that an increase in hardness in the region with a maximum temperature and plasma jet tempering is caused by redistribution of carbon from the carbide phases into martensite [3]. The hardened zone in all the samples has the identical structure, consisting of segments of different sizes and a dark spot. The presence of three zones is a result of tempering effect of the plasma jet. An increase in size and amount of ferrite and individual inclusions of δ-ferrite (δ-F) are seen in some regions of the hardened layers, which is associated with overheating of steel. An increase in the heat flow and power concentration is accompanied by a decrease in length of the hardened and transition zones and an increase in hardness, which is likely to be associated with crushing of martensite blocks and other phenomena related to phase cold-work hardening. By selecting the travel speed of the plasmatron and the value of overlap of a segment, it is possible to produce a structure with maximum wear and corrosion resistance, which is important for operation in aggressive environments. Precipitation of undesirable phases in plasma hardening can be prevented by varying the hardening parameters and location of the sprayers.

REFERENCES

1. Leshchinsky, L.K., Camotugin, S.S., Pirch, I.I. *et al.* (1990) *Surface plasma hardening*. Kyiv: Tekhnika.
2. Karpov, L.P. (1993) Effect of quenching conditions on carbide network in steel 07Kh16N6. *Metallovedeniye i Term. Obrabotka Metallov*. **1**, 13 – 15.
3. Blanter, M.E. (1962) *Phase transformations in heat treatment of steel*. Moscow: Goschertsvetmet.

DIMENSIONS OF THE ZONE OF BOILER WALLS CLEANING FROM SOLIDIFIED PITCH IN WELDING UP CRACKS

A.M. BERESTOVOY
Priazov State Technical University, Mariupol, Ukraine

ABSTRACT

Sizes of the zones to be cleaned from pitch for repair welding of cracks formed during operation in the tank boilers were established experimentally using simulation samples. The possibility of avoiding overall cleaning of the tank boiler is proved. The technology for repair welding of cracks eliminating inflammation of pitch is described.

Key words: *repair welding, welding up cracks, low-alloyed steel, boiler of tank car, cleaning from pitch.*

During operation of tank cars with electrical heating [1], which transport high-temperature (80 – 300 °C) solidifying liquids, in particular coal-tar pitch and natural sulphur, it was found that in the zones of more intensive heating of the lower part of the boiler (with heaters located under the boiler), the boiler walls are prone to irreversible deformations in the form of «buckling» outside of the boiler, in the presence of a hard refractory precipitate on them. They are especially often found in the zones of active heating in the middle part of the boiler lower zone between the legs of its fastening to the frame, as well as between the boiler legs and its extreme supports. Buckling areas can be more than one square meter, and during their development, 500 to 600 mm long through-thickness cracks can initiate in them [2]. Process repair of such tank cars is rather labour-consuming as it requires complete dismantling of the part of the tank car above the platform.

Theoretical and experimental studies [3] were conducted, in order to determine the ability to repair the boiler in operation without complete cleaning of its internal surface from the liquid solidified on its walls and without dismantling the thermal insulation or the system of the tank car electric heating. In this case the goal was to determine the dimensions of the zones of the boiler walls cleaning from solidified liquid only in the places of welding up the cracks from the boiler inner side.

Investigation of the degree of cleaning from pitch and dimensions of the boiler wall area to be cleaned for welding up a crack in tank cars not cleaned from the remnants of the pitch, envisages determination of the dimensions of a zone clean from pitch around the crack, proceeding from the admissible temperature of the boiler wall, which eliminates pitch ignition and evolution of harmful substances. The ignition temperature of medium-temperature pitches is equal to 200 to 250 °C [4]. For investigation purposes the temperature of ignition of the pitches and their precipitates is assumed to be equal to 250 °C.

Theoretical investigations included calculation of the welding modes and establishment of the temperature zones around the weld, and experimental studies consisted in welding up cracks in the boiler sheet which had a layer of coal-tar pitch.

In order to determine the minimal zone of cleaning the boiler wall from the pitch solidified on it or its precipitates, it is necessary to calculate temperature distribution along the weld (along x axis) and normal to the direction of welding (along y axis) in welding up boiler cracks. In crack welding up in one pass with complete penetration, the same temperatures across thickness δ of the plates being welded can be assumed. In this case, the electric welding arc is a linear heat source distributed across the thickness.

The temperature of the body heating by this heat source was determined by the procedure from [5]. When a layer of solidifying liquid is present on the metal surface, coefficient α of convective heat transfer changes, and its value was determined by the procedure of [6]. If the pitch layer is on one side of the plate, the total coefficient α of convective heat transfer consists of the coefficient α_m of heat transfer from the metal surface and coefficient α_p of heat transfer through a layer of pitch.

Experimental research was performed in order to determine the possibility of tank car repair (welding up cracks) with partial removal of pitch from them. The research was conducted under laboratory conditions at ambient temperature of 18 °C on a boiler wall simulator with 5 to 10 mm thick layer of pitch from both sides. The simulator was a plate of 500×500 mm size of a full thickness of the boiler wall ($\delta = 12$ mm). Plate material was low-alloyed 09G2SD steel actually used for manufacture of the boiler of a tank car for transportation of coal-tar pitch. Three variants of possible defects and of their repair by welding were reproduced in the simulator, namely weld bead deposition on metal without cracks, simulating welding (in repair) to the boiler walls of some parts of its internal fixtures (for instance, fasteners of inlet-outlet pipes); welding up from both sides of a through-thickness crack which had violated the tightness of the internal cavity of the tank car boiler; welding up from one side of a not through-thickness crack on the boiler wall, which developed at the initial stage of defect formation or welding up of the end sections of the through-thickness crack.

In the zone of deposition of 25 to 30 mm wide weld the simulator metal was cleaned from the pitch layer mechanically (with scrapers and sand paper) to metallic lustre.

Crack welding up was performed on the entire length of the simulator with 5 mm diameter electrodes of E42A UP-1/45 type. Cracks preparation for welding and the technology of welding operations performance were in keeping with the current standards on repair by welding of the rolling stock of the railways [7]. Experimental testing conducted in the simulator was assessed visually and the results were photographed. The graphotopological portrait of the welding zone with its temperature indices was made [3].

The conducted experimental and theoretical investigations gave rise to the following conclusions: in welding up of cracks on the wall of the tank car boiler which has a layer of solidified pitch on it, the wall should be cleaned from pitch at a distance of not less than 50 to 75 mm and not more than 100 mm from the longitudinal axis of the weld, this eliminating pitch ignition in cracks welding up and preventing the evolution of vapors harmful for man from it. In this case, however, the zones adjacent to the weld which are not cleaned from pitch, should be covered by non-inflammable materials, for instance, asbestos, or water-impregnated textiles, which protect the uncleaned zones with pitch from the molten metal spatter flying out in welding.

The theoretical and experimental investigations performed for the case of tank cars for transportation of coal-tar pitch, enabled development of specifications on crack welding up under the conditions of service [8].

The investigation results are used in a centralized depot for repair of tank cars for pitch in the Sayanogorsk Aluminium Factory (Krasnoyarsk region), as well as in the factories of the aluminium industry when coal-tar pitch in the molten condition is transported in tank cars [9].

REFERENCES

1. Ivanchenko, G.S., Berestovoy, A.M. (1973) Railway tank car for transportation of solidifying liquids. In: *Col. of pap. of Experience of innovators of Zhdanov Heavy Engineering Factory*. Moscow: Niiinformtyazhmash.
2. (1983) *Analysis of the technical condition and repairability of thermal tank cars for pitch in service*. Moscow: MTsM.
3. (1986) Development and introduction of a set of measures on organization of operation and repair of special-purpose railway rolling stock in industrial transport of VPO Zoyuzaluminiy. In: *NIR-1986 report Zhdanov MI*. Zhdanov: Zhdanovtyazhmash.
4. Privalov, V.E., Stepanenko, M.A. (1981) *Coal-tar pitch: production, processing, application*. Moscow: Metallurgia.
5. Bagryansky, K.V. (1976) *Theory of welding processes*. Kyiv: Vyshcha Shkola.
6. (1978) *Tank car for pitch, 15-1532 model. Calculation of technico-economical parameters.* Mariupol: Zhdanovtyazhmash.
7. (1978) *Manual on welding and surfacing in repair of carriages and containers. RTM 32 TsV 201–78*. Moscow: Transport.
8. (1988) *Industry specifications on depot repair of a tank car for pitch of model 15-1532. TU 22-2-25*.
9. (1988) *Industry specification for overhauling of a tank car for pitch of model 15-1532. TU 22-2-26*.

PORTABLE MECHANICAL DEVICES FOR CUTTING AND PREPARATION OF PIPES FOR WELDING

V.D. KOVALYOV, N.M.VASHCHENKO and A.G.TARASENKO
The E.O. Paton Electric Welding Institute, NASU, Kyiv, Ukraine

ABSTRACT

Pneumatic portable metal-cutting machine-tools for cutting pipes of diameter from 20 to 1220 mm in site and pipe facing for welding are described. Portable pipe cutting and facing machines can be used in manufacture and repair of pipelines. Unique designs of captive non-detachable pipe cutters are given.

Key words: *repair of pipelines, pipe cutters, facing machines, cutting and facing of pipe, boiler construction, heat and nuclear power engineering.*

During recent years the portable mechanical cutting devices of an orbital type for pipe cutting, i.e. pipe cutters, are widely used in the world practice in manufacture and repair of the pipelines. As compared with heat and abrasive methods of pipe cutting the mechanical pipe cutters provide the accuracy of a cut and pipe perpendicularity. This contributes to the accuracy in subsequent abutting of pipes and 100 % automation of welding, thus providing its high quality.

Using pipe cutters, it is possible to cut out the areas of pipelines to be repaired in hard-to-reach places in all spatial positions. For this, the operator has to fasten the pipe cutter on a pipe, and then the cutting is performed automatically without his participation. The pipe cutters are also used for chamfering the pipe ends for welding, for external and internal grooving of pipe ends.

Other mechanical devices, such as facing machines, are also convenient in operation. They are used for pipe end facing for welding in site, in repair works, in stationary conditions for the pipe preparation for welding.

In Ukraine the pipe cutting and facing machines of both domestic and foreign companies, such as «TRI TOOL» and «Wachs» (USA), «Protem» (France), «Babcock» (UK) and «Siemens» (Germany) are used.

The fields of application of portable pipe cutters and facing machines are very wide: boiler and pipe industries, construction and repair of gas and oil pipelines, site and repair works in heat and, in particular, nuclear stations.

Below, some design features of domestic pipe facing machines will be described.

Pipe facing machine TT 160 (Figure 1) is a portable metal-cutting machine designed for preparation of ends of position pipes, made from low-alloyed, medium-alloyed and stainless steels, for welding. They can also perform inner and external grooving of the pipe end for a length of not more than 25 mm. Drive of this facing machine, located along the pipe axis, is a pneumatic motor with a planetary reduction gear. This facing machine is centered and clamped on the pipe with the help of an inner-pipe unclamping collet with three changeable wedges. Two cutters, similar in shape to a chamfer for welding, are fixed on a rotating faceplate.

Pipe facing machine TF 110 has a similar design but a pneumatic drive is located normal to the axis of the pipe to be faced that it is convenient in operation in hard-to-reach places.

Technical characteristics of the pipe facing machine are given in Table 1.

All the pipe cutters have a design which allow them to be mounted on an infinite pipe. Drive is a pneumatic or hydraulic motor with a planetary reduction gear. Two screwed supports with cutter-holders, in which cutters are fixed, are fastened on a rotating faceplate. Sprockets, whose teeth are run over the fixed rests, for rotating the support screws per a pitch of cutters feeding, are fastened

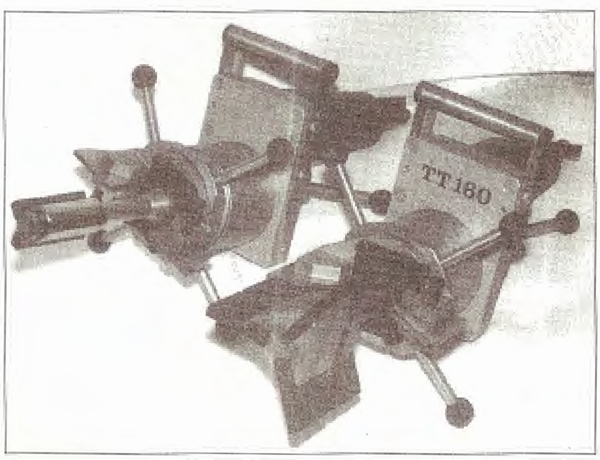

Figure 1. Pipe facing machine TT 160.

Figure 2. Fastening of a detachable pipe cutter on a pipe to be cut.

at the ends of the screws. Thus, the whole thickness of the pipe is cut.

Pipe cutters are divided, by the method of their fastening on the pipe, into detachable and non-detachable.

The detachable pipe cutters before their setting on an infinite pipe should be completely dismantled and then assembled on the pipe at the spot of welding. Screw rests are used for centering the pipe cutters on the pipe. Domestic pipe cutters of a series TrR 89-820 are given in Table 2, and those of company «Wachs» are shown in Figure 2.

The drawback of the detachable pipe cutters is their assembly which takes much time that is inadmissible in repair of pipelines at the nuclear stations.

Table 1. Technical characteristics of pipe facing machines*

Facing machine	*Range of ID, mm*	*Wall thickness, mm*	*Power of pneumatic motor, kW*	*Mass, kg*
TT 160	40 – 160	1.5 – 12.0	1.60	16.5
TF 110	20 – 100	1.5 – 9.0	1.25	10.6

*Facing machines of both types have 2 cutters, faceplate rotation is 33 rpm, compressed air pressure is 0.4 – 0.6 MPa, axial feeding of cutters is 25 mm.

This drawback is less pronounced in hinge-opening pipe cutters. These are pipe cutters of company «Wachs» for large-diameter pipes used mainly for transportation of oil and gas and also our domestic pipe cutter TrR 820-1220 used in construction and repair of main pipelines. To be installed on the pipe the two halves of the pipe cutter body are hinge-open by a screw which has a left-hand and right-hand thread and interacts with corresponding nuts on the body halves. The ends of the pipe cutter body are fastened by a screw with a nut located at the ends of the body halves. Centering on the pipe is performed with four separate run-out screw rests. Undoubtedly, this design also requires a comparatively much time for fastening and centering of the pipe cutter.

To reduce to maximum the time of installing the pipe cutter on the pipe, non-detachable pipe cutters TrN 38-76 and TrN 80-219 of a general purpose and special pipe cutters TrTs 57 (Figure 4) and RTK 70 (Table 2) which have no foreign analogues, have been developed. As the bodies and faceplates of these pipe cutters are made with a side slot they can be put on the pipe from the side and clamped with the help of converging centering prisms. The cutters feeding is also automatic as in detachable pipe cutters.

Table 2. Technical characteristics of pipe cutters*

Pipe cutter	*OD of pipes, mm*	*Wall thickness, mm*	*Power of pneumatic motor, kW*	*Cutting speed, m/min*	*Pitch of cutter feeding, mm*	*Method of clamping on pipe*	*Mass, kg*
				Detachable			
TrR 89-820	89, 108, 160, 219, 325, 426, 820	4.0 – 25.0	3.00	10.2 – 13.8	0.05 – 0.08	Screw rests	36.0 – 234.0
TrR 820-1220	820, 1020, 1220	4.0 – 25.0	3.00	13.5 – 20.0	0.08	Same	138.0 – 256.0
				Non-detachable			
TrN 38-76	38 – 76	1.0 – 10.0	1.60	4.9 – 10.0	0.08	Manual, with prisms	28.0
TrN 80-219	80 – 219	3.0 – 18.0	1.60	4.9 – 10.0	0.07	Same	32.0 – 54.0
TrTs 57	57 ± 1	1.5 – 10.0	1.25	6.0 – 13.0	0.08	Pneumatic, with levers	11.3
RTK 70	56 – 70	1.5 – 12.0	1.25	6.0 – 13.0	0.08	Same	10.2

*Compressed air pressure in all types of pipe cutters is 0.4 – 0.6 MPa, number of cutters is 2, frequency of faceplate rotation in TrN 38-76 is 33 ± 10 rpm; TrN 80-219 is 46 ± 10 rpm; TrTs 57 is 60 ± 10 rpm ; RTK 70 is 50 ± 10 rpm.

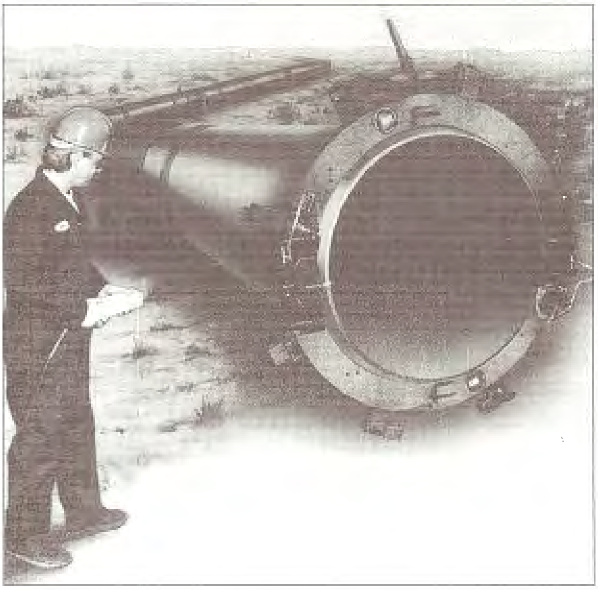

Figure 3. Pipe cutter TrR 820-1220.

Special non-detachable pipe cutters TrTs 57 and RTK 70, first of them was implemented at Chernobyl NPS, can reduce by 10 – 15 times the doses of personnel radiation at a regular repair for replacement of pipings in the under-reactor room. They have pneumatic drives of an increased reliability, the cutters are fed automatically and faceplates are made with side slots. They are featured by a unique quick-response air-operated lever-type clamp with a mechanical blocking allowing the pipe cuter to be attended by one operator and to be installed and removed (in the zone of a high radiation) for 30 – 40 s.

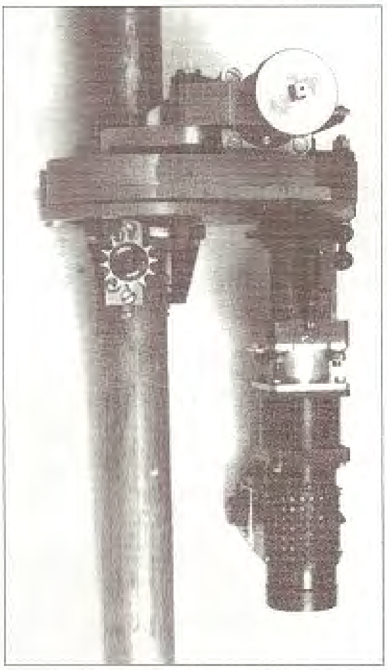

Figure 4. Air-operated pipe cutter TrTs 57.

Time of automatic cutting of pipe of 57 mm diameter, 4.5 mm thickness is not more than 1.5 min.

The design of these pipe cutters is unique and protected by a patent of Ukraine.

It should be noted in conclusion that the most part of the above-mentioned devices for the preparation of pipes, developed at the E.O. Paton Electric Welding Institute, was manufactured and implemented at the power engineering enterprises.